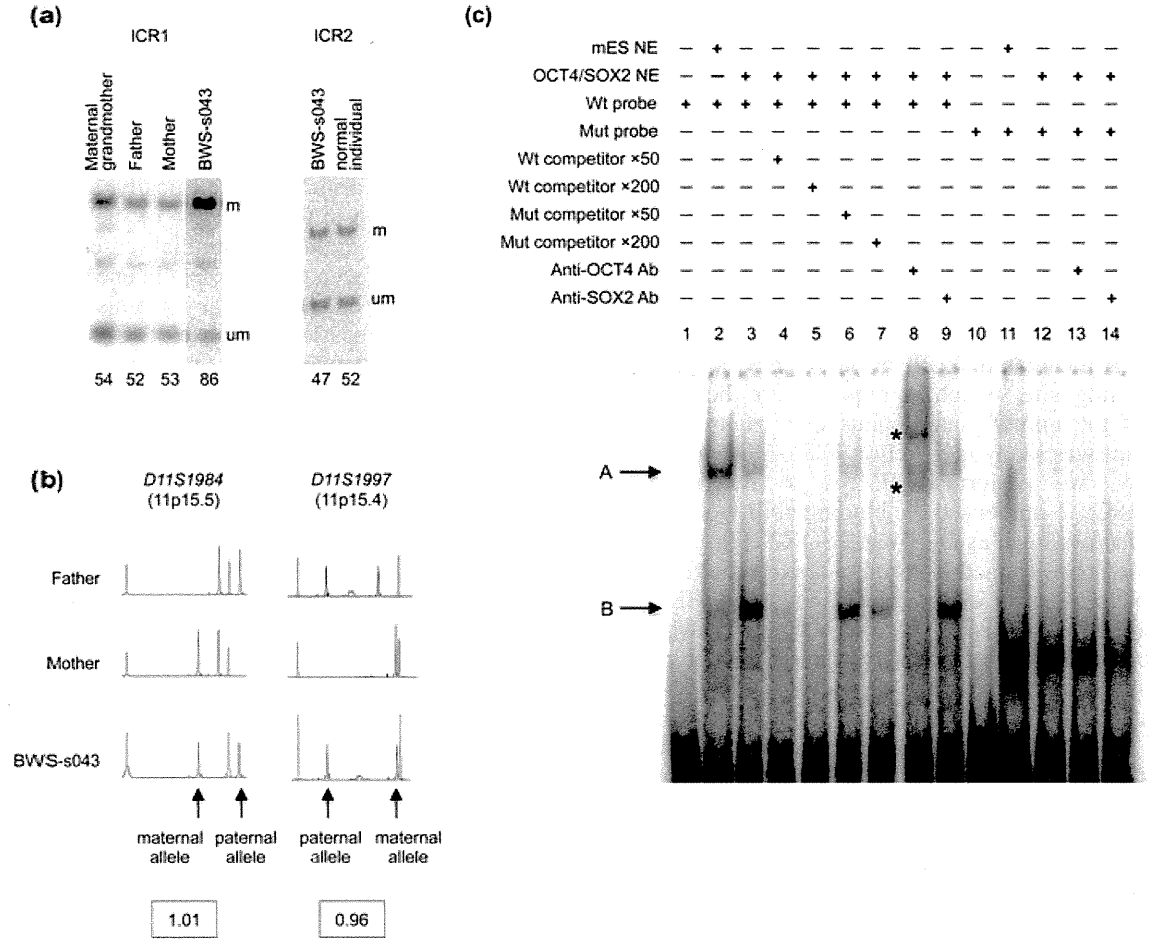

Fig. 2. Methylation-sensitive Southern blots and microsatellite analysis of BWS-s043, and electrophoretic mobility shift assay (EMSA) for 2,023,018C>T. (**a**) Methylation-sensitive Sothern blots of ICR1 and ICR2. Methylation indices [MI, %] are shown below each lane. MI was calculated using the equation $M/(M+U) \times 100$, where M is the intensity of the methylated band and U is the intensity of the unmethylated band. m, methylated band; um, unmethylated band. BWS-s043 showed ICR1-GOM, whereas the relatives did not. Methylation statuses of CTS1 and CTS4 are shown in Fig. S2b,c. Methylation of ICR2 in BWS-s043 was normal. (**b**) Microsatellite analysis at 11p15.4-p15.5. Ratios of the paternal allele to the maternal allele in BWS-s043 were approximately 1, indicating no uniparental disomy. Red peaks are molecular markers. (**c**) EMSA using the wild-type (Wt) probe and the mutant (Mut) probe encompassing 2,023,018C>T. The unlabeled Wt probe or Mut probe (×50 or ×200 molar excess) was used as a competitor. The arrows and asterisks indicate the protein-DNA complexes (A and B) and supershifted complexes, respectively. mES NE, nuclear extract from mouse ES cells; OCT4/SOX2 NE, nuclear extract from human HEK293 cells expressing OCT4/SOX2; Ab, antibody.

for BWS-s043, were not located at any protein-binding sites that have been reported as involved in methylation imprinting (CTCF, OCT, and ZFP57) (3, 4, 10, 12, 16). Furthermore, we did not find any protein-oligonucleotide complexes in EMSA using mouse ES nuclear extracts and oligonucleotide probes encompassing all variants, except for BWS-s043 (Fig. S1). Therefore, we analyzed further three variants in BWS-s043, which were in and around the OCT-binding site 1.

First, we re-confirmed that BWS-s043 showed GOM near CTS6 within ICR1, but it did not demonstrate LOM at ICR2, paternal uniparental disomy of chromosome 11, or a *CDKN1C* mutation (Fig. 2a,b, and data not shown). The 2,023,018C>T variant was located in the second octamer motif of OCT-binding site 1 within repeat A2 (Fig. 1a). The other two variants were located approximately 450 bp on the telomeric side of the 2,023,018C>T variant, between repeats A2 and B4 (Fig. 1a, Table 1). The 2,023,018C>T variant was absent in other family members, indicating a *de novo* variant (Fig. 1a). To clarify if the *de novo* variant in the patient occurred on the maternal or paternal allele, we performed haplotype analysis with PCR covering all three variants. We found all three variants were located on the same allele and the 2,023,018C>T variant occurred *de novo* on the maternal allele because the 2,022,561–562CT>delCT and 2,022,565G>C variants were on the maternal allele in the patient (Fig. 1b,c).

Next, we investigated the methylation status of ICR1. Methylation-sensitive Southern blots and bisulfite sequencing showed normal methylation of ICR1 in the parents and the maternal grandmother (Figs 2a and S2). As for the 2,022,561-562CT>delCT and the 2,022,565G>C variants, the variant allele was unmethylated in the mother, but methylated in the grandmother (Fig. 1d). On the basis of methylation

analysis, the variant allele in the grandmother must have been transmitted by her father, and that in the mother must have been transmitted by her mother. The results indicated that the variant allele could be either methylated or unmethylated during gametogenesis, strongly suggesting no relation between the variants and ICR1-GOM. On the other hand, bisulfite sequencing including the 2,023,018C>T variant revealed that both the variant and wild-type alleles were heavily methylated in the patient (Fig. 1e), while differential methylation was maintained in other family members and normal controls without the variant (Fig. S2a). As the *de novo* variant on the maternal allele was located within the OCT-binding site, which is required for the maintenance of the unmethylated status in a mouse model, the variant was likely involved in ICR1-GOM (17, 18).

Finally, we performed EMSA to determine if 2,023,018C>T influenced the binding ability of nuclear protein factors, such as OCT4 and SOX2 (Fig. 2c). The wild-type probe formed two complexes (A and B) with the nuclear extracts of mouse ES cells and HEK293 cells expressing OCT4/SOX2 (lanes 2 and 3), whereas such complexes were not observed in the mutant probe (lanes 11 and 12). Complexes A and B competed more efficiently with wild-type than with the mutant competitor (lanes 4 to 7). Furthermore, complex B, but not A, was supershifted with the antibody against OCT4 (lane 8). The supershift did not occur with the antibody against SOX2 and with both antibodies using the mutant probe (lanes 9, 13, and 14). These data demonstrated that 2,023,018C>T abrogated binding ability of a nuclear factor, most likely OCT4. Taken together, our data strongly suggest that 2,023,018C>T is a mutation that could prevent OCT4 binding to the OCT-binding site and induce ICR1-GOM, leading to BWS.

Discussion

We identified a novel *de novo* point mutation, chr11: 2,023,018C>T, in OCT-binding site 1 within repeat A2 in a BWS patient with ICR1-GOM. Our data strongly suggest the involvement of the mutation in GOM at ICR1. In a mouse cell model, the evolutionarily well-conserved dyad octamer motif within ICR1, which is bound by OCT protein, has been shown to be required for the maintenance of unmethylated status competing against *de novo* methylation (17). In addition, the importance of a SOX motif flanked by an OCT motif has also been reported (19). Recent studies have shown that the SOX–OCT motif functions to maintain unmethylated status *in vitro* and *in vivo*; a cooperative function of CTCF and OCT/SOX for maintenance of differential methylation has been suggested as responsible (18, 19). Although there is one OCT-binding site in mice, three evolutionarily conserved OCT-binding sites (0, 1, 2) are located in and around ICR1 in humans. As all mutations and the small deletion previously reported in addition to our case occurred in site 1 within repeat A2 (Fig. 1a), site 1 within repeat A2 likely plays a more important role for maintaining unmethylated status of maternal ICR1 in humans than the other OCT-binding sites (10, 12, 13).

ICR1-GOM cases, including ours, with mutations/deletions also show partial hypermethylation in spite of pre-existent genetic aberrations in the oocyte (9, 12, 13, 20), suggesting aberrant hypermethylation at ICR1 would also be stochastically acquired at a cellular level even in the existence of such aberrations.

As for SRS, including familial cases, the ICR1 mutation has not been found except in one sporadic case to date (10). We did not find any promising mutations in this study, suggesting the cause of ICR1 methylation defects to differ between SRS and BWS.

In conclusion, we identified a novel *de novo* point mutation of OCT-binding site 1 within repeat A2, a location suggested to play an important role for maintaining the unmethylated status of maternal ICR1 in humans, on the maternal allele in a BWS patient with ICR1-GOM. However, genetic aberrations of ICR1 explain only 20% of BWS cases with ICR1-GOM (10). As aberrant methylation may occur as a consequence of stochastic events or environmental influences irrespective of ICR1 mutations, unknown causes for ICR1 methylation defects should be clarified.

Supporting Information

The following Supporting information is available for this article:

Fig. S1. EMSA for all variants found in this study, except for those in BWS-047 and BWS-s061, using the nuclear extract from mouse ES cells. The variant in BWS-s081 was located outside of ICR1, and a CpG site within the probe sequence was mostly unmethylated in three normal controls (data not shown). Thus, an unmethylated probe was used for it. Since the variants in BWS-s100 and SRS-s03 were located 3′ of CTS6 and found on the maternal allele, unmethylated probes were used for them. As for the variant in SRS-002, it was located 5′ of CTS1 but its parental origin was unknown. Thus, both unmethylated and methylated probes were used for it. There was no difference between a wt-probe and a variant-probe in each variant except for the BWS-s043 mutation. A wt-probe for the BWS-s043 mutation formed two complexes, whereas such complexes were not observed with a probe for the mutation. These results suggested that only the BWS-s043 mutation affected the protein–DNA interaction (see text and Fig. 2c for details). WT, probe for the wild-type sequence; MUT, probe for the BWS-s043 mutation; VAR, probe for the variant sequence; um, unmethylated probe; me, methylated probe; mES NE, nuclear extract from mouse ES cells.
Fig. S2. Bisulfite sequencing of the region encompassing the 2,023,018 variant, CTS1, and CTS4. (**a**) Results for the 2,023,018 variant. In the healthy members of the BWS-s043 family, comprised of the maternal grandmother, mother, and father, showed differential methylation. Three normal controls also showed differential methylation. In particular, normal control 3 was heterozygous for a SNP (rs61520309) and showed differential methylation in an allele-dependent manner. Open and filled circles indicate unmethylated and methylated CpG sites, respectively. (**b**) Results for CTS1. Two normal controls that were heterozygous for a SNP (rs2525885) showed differential methylation. The healthy family members also showed differential methylation, whereas the patient, BWS-s043, showed aberrant hypermethylation. CpG sites within CTS1 are indicated by a short horizontal line. X indicates T of the SNP (rs2525885). (**c**) Results for CTS4. The healthy family members and two normal controls showed differential

methylation. Among them, the parents and two normal controls were heterozygous for a SNP (rs2525883). The patient, BWS-s043, showed aberrant hypermethylation. CpG sites within CTS4 were indicated by a short horizontal line. X indicates T of the SNP (rs2525883).
Table S1. PCR primers and oligonucleotide probes used in this study.

Additional Supporting information may be found in the online version of this article.

Acknowledgements

This study was supported, in part, by a Grant for Research on Intractable Diseases from the Ministry of Health, Labor, and Welfare; a Grant for Child Health and Development from the National Center for Child Health and Development; a Grant-in-Aid for Challenging Exploratory Research; and, a Grant-in-Aid for Scientific Research (C) from the Japan Society for the Promotion of Science.

References

1. Weksberg R, Shuman C, Beckwith JB. Beckwith–Wiedemann syndrome. Eur J Hum Genet 2010: 18: 8–14.
2. Gicquel C, Rossignol S, Cabrol S et al. Epimutation of the telomeric imprinting center region on chromosome 11p15 in Silver–Russell syndrome. Nat Genet 2005: 37: 1003–1007.
3. Bell AC, Felsenfeld G. Methylation of a CTCF-dependent boundary controls imprinted expression of the Igf2 gene. Nature 2000: 405: 482–485.
4. Hark AT, Schoenherr CJ, Katz DJ, Ingram RS, Levorse JM, Tilghman SM. CTCF mediates methylation-sensitive enhancer-blocking activity at the H19/Igf2 locus. Nature 2000: 405: 486–489.
5. Schoenherr CJ, Levorse JM, Tilghman SM. CTCF maintains differential methylation at the Igf2/H19 locus. Nat Genet 2003: 33: 66–69.
6. Pant V, Mariano P, Kanduri C et al. The nucleotides responsible for the direct physical contact between the chromatin insulator protein CTCF and the H19 imprinting control region manifest parent of origin-specific long-distance insulation and methylation-free domains. Genes Dev 2003: 17: 586–590.
7. Sparago A, Cerrato F, Vernucci M, Ferrero GB, Silengo MC, Riccio A. Microdeletions in the human H19 DMR result in loss of IGF2 imprinting and Beckwith–Wiedemann syndrome. Nat Genet 2004: 36: 958–960.
8. Prawitt D, Enklaar T, Gärtner-Rupprecht B et al. Microdeletion of target sites for insulator protein CTCF in a chromosome 11p15 imprinting center in Beckwith–Wiedemann syndrome and Wilms' tumor. Proc Natl Acad Sci U S A 2005: 102: 4085–4090.
9. Beygo J, Citro V, Sparago A et al. The molecular function and clinical phenotype of partial deletions of the IGF2/H19 imprinting control region depends on the spatial arrangement of the remaining CTCF-binding sites. Hum Mol Genet 2013: 22: 544–557.
10. Demars J, Shmela ME, Rossignol S et al. Analysis of the IGF2/H19 imprinting control region uncovers new genetic defects, including mutations of OCT-binding sequences, in patients with 11p15 fetal growth disorders. Hum Mol Genet 2010: 19: 803–814.
11. Quenneville S, Verde G, Corsinotti A et al. In embryonic stem cells, ZFP57/KAP1 recognize a methylated hexanucleotide to affect chromatin and DNA methylation of imprinting control regions. Mol Cell 2011: 44: 361–372.
12. Poole RL, Docherty LE, Al Sayegh A et al. Targeted methylation testing of a patient cohort broadens the epigenetic and clinical description of imprinting disorders. Am J Med Genet A 2013: 161: 2174–2182.
13. Berland S, Appelbäck M, Bruland O et al. Evidence for anticipation in Beckwith–Wiedemann syndrome. Eur J Hum Genet 2013: 21: 1344–1348.
14. Higashimoto K, Nakabayashi K, Yatsuki H et al. Aberrant methylation of H19-DMR acquired after implantation was dissimilar in soma versus placenta of patients with Beckwith–Wiedemann syndrome. Am J Med Genet A 2012: 158A: 1670–1675.
15. Soejima H, Nakagawachi T, Zhao W et al. Silencing of imprinted CDKN1C gene expression is associated with loss of CpG and histone H3 lysine 9 methylation at DMR-LIT1 in esophageal cancer. Oncogene 2004: 23: 4380–4388.
16. Mackay DJ, Callaway JL, Marks SM et al. Hypomethylation of multiple imprinted loci in individuals with transient neonatal diabetes is associated with mutations in ZFP57. Nat Genet 2008: 40: 949–951.
17. Hori N, Nakano H, Takeuchi T et al. A dyad Oct-binding sequence functions as a maintenance sequence for the unmethylated state within the H19/Igf2-imprinted control region. J Biol Chem 2002: 277: 27960–27967.
18. Sakaguchi R, Okamura E, Matsuzaki H, Fukamizu A, Tanimoto K. Sox-Oct motifs contribute to maintenance of the unmethylated H19 ICR in YAC transgenic mice. Hum Mol Genet 2013: 22: 4627–4637.
19. Hori N, Yamane M, Kouno K, Sato K. Induction of DNA demethylation depending on two sets of Sox2 and adjacent Oct3/4 binding sites (Sox-Oct motifs) within the mouse H19/insulin-like growth factor 2 (Igf2) imprinted control region. J Biol Chem 2012: 287: 44006–44016.
20. Sparago A, Russo S, Cerrato F et al. Mechanisms causing imprinting defects in familial Beckwith–Wiedemann syndrome with Wilms' tumour. Hum Mol Genet 2007: 16: 254–264.

Rumbajan et al. BMC Cancer 2013, 13:608
http://www.biomedcentral.com/1471-2407/13/608

BMC Cancer

RESEARCH ARTICLE Open Access

Comprehensive analyses of imprinted differentially methylated regions reveal epigenetic and genetic characteristics in hepatoblastoma

Janette Mareska Rumbajan[1,2], Toshiyuki Maeda[1], Ryota Souzaki[3], Kazumasa Mitsui[4], Ken Higashimoto[1], Kazuhiko Nakabayashi[5], Hitomi Yatsuki[1], Kenichi Nishioka[1], Ryoko Harada[4], Shigehisa Aoki[6], Kenichi Kohashi[7], Yoshinao Oda[7], Kenichiro Hata[5], Tsutomu Saji[4], Tomoaki Taguchi[3], Tatsuro Tajiri[8], Hidenobu Soejima[1*] and Keiichiro Joh[1*]

Abstract

Background: Aberrant methylation at imprinted differentially methylated regions (DMRs) in human 11p15.5 has been reported in many tumors including hepatoblastoma. However, the methylation status of imprinted DMRs in imprinted loci scattered through the human genome has not been analyzed yet in any tumors.

Methods: The methylation statuses of 33 imprinted DMRs were analyzed in 12 hepatoblastomas and adjacent normal liver tissue by MALDI-TOF MS and pyrosequencing. Uniparental disomy (UPD) and copy number abnormalities were investigated with DNA polymorphisms.

Results: Among 33 DMRs analyzed, 18 showed aberrant methylation in at least 1 tumor. There was large deviation in the incidence of aberrant methylation among the DMRs. *Kv*DMR1 and *IGF2*-DMR0 were the most frequently hypomethylated DMRs. *INPP5Fv2*-DMR and *RB1*-DMR were hypermethylated with high frequencies. Hypomethylation was observed at certain DMRs not only in tumors but also in a small number of adjacent histologically normal liver tissue, whereas hypermethylation was observed only in tumor samples. The methylation levels of long interspersed nuclear element-1 (LINE-1) did not show large differences between tumor tissue and normal liver controls. Chromosomal abnormalities were also found in some tumors. 11p15.5 and 20q13.3 loci showed the frequent occurrence of both genetic and epigenetic alterations.

Conclusions: Our analyses revealed tumor-specific aberrant hypermethylation at some imprinted DMRs in 12 hepatoblastomas with additional suggestion for the possibility of hypomethylation prior to tumor development. Some loci showed both genetic and epigenetic alterations with high frequencies. These findings will aid in understanding the development of hepatoblastoma.

Keywords: Hepatoblastoma, Genomic imprinting, Differentially methylated region, DNA methylation

Background

Hepatoblastoma is the most common primary liver tumor in children, accounting for just over 1% of pediatric cancers and 79% of liver cancers in children under the age of 15 [1]. Most of these tumors are purely derived from epithelium composed exclusively of immature hepatocytic elements, known as fetal and embryonal types. The fetal type consists of smaller than normal hepatocytes that are arranged in irregular laminae, recapitulating those of the fetal liver. The embryonal type is comprised of smaller cells as compared to the fetal type. It has a more immature appearance and pattern of growth. Some of the tumors, referred to as mixed type, are characterized by epithelial patterns and spindled mesenchymal cells. A much rarer variant of such mixed type tumor harbors teratoid features, which contains foci of mature cartilage, intestinal-type or keratinized epithelium, melanin pigment, or skeletal

* Correspondence: soejimah@cc.saga-u.ac.jp; joh@cc.saga-u.ac.jp
[1]Department of Biomolecular Sciences, Division of Molecular Genetics & Epigenetics, Faculty of Medicine, Saga University, Nabeshima 5-1-1, Saga 849-8501, Japan
Full list of author information is available at the end of the article

muscle in addition to the elements mentioned above. To date, several genetic and epigenetic features have been observed in hepatoblastoma (reviewed in [2]). The most recurrent cytogenetic abnormalities include the presence of extra copies of chromosomes 2, 8, 20, and the loss of chromosome 4. Mutations or upregulation of the genes involved in embryonic development have been reported. For example, *APC*, *CTNNB1*, *AXIN1*, and *AXIN2* (key factors involved in the Wnt signaling pathway) are frequently mutated, suggesting that aberration of this pathway occurs as an early event during tumorigenesis. Mutation of *PIK3CA*, amplification of *PIK3C2B*, and upregulation of hedgehog ligands and their target genes have also been reported. Epigenetic silencing by promoter hypermethylation occurs at several tumor suppressor genes, such as *SFRP1*, *APC*, *HHIP*, *SOCS1*, *CASP8*, and *RASSF1A*. In addition, several imprinted genes, including *IGF2*, *DLK1*, *PEG3*, *PEG10*, *MEG3*, and *NDN*, have been reported to be overexpressed in hepatoblastoma [2].

Imprinted genes are expressed in a parent-of-origin-specific manner. They are usually clustered in subchromosomal regions called imprinting domains. The human genome contains more than 30 imprinting domains (http://www.geneimprint.com). Imprinting domains have at least one DMR that are characterized by DNA methylation on one of the two parental alleles. There are maternally methylated DMRs and paternally methylated DMRs. In addition, two classes of imprinted DMRs, gametic and somatic, have been described. Gametic DMRs acquire methylation during gametogenesis and the methylation is maintained from zygote to somatic cells during all the developmental stages. Most gametic DMRs are known as imprinting control regions (ICRs) that regulate the imprinted expression of the genes in the domain. By contrast, methylations of somatic DMRs are established during early embryogenesis after fertilization under the control of nearby ICRs [3]. Somatic DMRs also regulate the expression of the imprinted genes.

Many imprinted genes regulate cell growth and differentiation, and, thus, disruption of imprinting, mainly due to aberrant DNA methylation at the responsible DMR, is implicated in pre- and/or post-natal growth disorders and in the pathogenesis of cancers [4]. For example, hypermethylation of *H19*-DMR, which is the ICR of the *IGF2/H19* imprinting domain at the 11p15.5 locus, is a cause of Beckwith-Wiedemann syndrome (BWS), the most common overgrowth syndrome characterized by occasional development of embryonal tumors, including hepatoblastoma [5]. The hypermethylation leading to biallelic expression of *IGF2* is seen in a range of tumors, also including hepatoblastoma [6,7]. The LOH of 11p15.5, especially the loss of the maternal allele, is found in approximately 20% of hepatoblastoma cases, and it is reported to be a risk factor for the relapse of this tumor [7,8]. Furthermore, several imprinted genes are overexpressed in hepatoblastoma as mentioned above. Thus, it is speculated that aberrant DNA methylation at imprinted DMRs is a key mechanism during malignant transformation of progenitor cells in a variety of tissues, including the liver [2,9]. However, the methylation status of imprinted DMRs scattered through the human genome has yet to be analyzed comprehensively in hepatoblastoma.

In this study, we performed comprehensive methylation analyses and polymorphism analyses of 33 imprinted DMRs in hepatoblastoma. We therefore describe some epigenetic and genetic characteristics of hepatoblastoma. These findings collectively aid in the understanding of the development of hepatoblastoma.

Methods

Samples

Twelve hepatoblastomas and their paired adjacent normal liver tissues were analyzed. Eleven sporadic hepatoblastoma samples (HB01 - HB11) were obtained from the Department of Pediatric Surgery, Faculty of Medicine, Kyushu University, Japan. One hepatoblastoma developed in a BWS patient (BWS109) was obtained from Toho University, Omori Medical Centre, Japan. Histochemical analyses of the tumor tissues indicated that the average of the tumor cell contents was approximately 70%. Ten of the patients were treated based on the Japanese Study Group for Pediatric Liver Tumor-2 (JPLT-2) protocol (HB08 and HB09 were not). Clinical information of the hepatoblastoma cases is shown in Table 1. Three livers (CL7, CL16, CBD1) were used as normal controls. CL7 (a 7-year-old who died from spinal muscular atrophy type I-C with chronic respiratory insufficiency) and CL16 (a 16-year-old who died after head trauma) were provided by the non-profit organization, Human & Animal Bridging Research Organization (Chiba, Japan). CBD1 (a 7-month-old who had congenital biliary dilatation) was obtained from the Department of Pediatric Surgery, Faculty of Medicine, Kyushu University. Written informed consents were obtained from the parents or the guardians of the participants, because the participants were children or dead. This study was approved by the Ethical Committee for Human Genome and Gene Analyses of the Faculty of Medicine, Saga University.

DNA isolation and bisulphite conversion

Genomic DNA was extracted from each sample using the QIAamp DNA Mini Kit (Qiagen, Germany) according to the manufacturer's instructions. One microgram of genomic DNA was subjected to bisulfite conversion using the EZ DNA Methylation Kit™ (Zymo Research, CA), and then the converted DNA was eluted in 100 μl of water.

Table 1 Clinical information of hepatoblastoma cases

Case	Sex/age[a]	Histology	PRETEXT	Preoperative chemotherapy[b]	POSTTEXT	Outcome	Other information
HB01	F/1y3m	Combined fetal and embryonal type	III	CITA4	III	Alive	
HB02	F/3y2m	Fetal type[c]	III	CITA4	III	Aive	
HB03	F/7y11m	Hepatoblastoma (NOS)[d]	III	CITA5	III	Alive	Small for gestational age
HB04	M/1y4m	Mixed epithelial and mesenchymal with teratoid feature[c]	IV	CITA4 + ITEC2	IV	Alive	
HB05	M/1y2m	Mixed epithelial and mesenchymal with teratoid feature	III	CITA5	II	Alive	
HB06	M/10m	Mixed epithelial and mesenchymal with teratoid feature	III	CITA4	III	Alive	
HB07	M/8m	Combined fetal and embryonal type	II	CITA2	II	Alive	
HB08	F/28d	Combined fetal and embryonal type	II			Alive	
HB09	M/1y6m	Combined fetal and embryonal type	II			Treatment related death	Small for gestational age
HB10	F/6y6m	Fetal type	II	CITA2	II	Alive	
HB11	F/3m	Combined fetal and embryonal type	IV	CITA7	III	Treatment related death	
BWS109	F/1y0m	Hepatoblastoma (NOS)[d]	IV,M(+)	CITA7 + ITEC1	IV	Alive	Beckwith-Wiedemann syndrome, liver transplantation at 1 year old

[a]age at diagnosis, [b]CITA: cisplatin-pirarubicin, ITEC: Ifosfamide, pirarubicin, etoposide, and carboplatin. The numerals indicate the cycle numbers of the chemotherapy. [c]difficult to diagnose due to chemotherapy, [d]not otherwise specified.

MALDI-TOF MS analysis

The methylation status of imprinted DMRs was screened by MALDI-TOF MS analysis with a MassARRAY system (Sequenom, CA) [10], according to the manufacturer's instructions. MALDI-TOF MS analysis produced signal pattern pairs indicative of non-methylated and methylated DNA. Epityper software analysis of the signals yielded the methylation index which ranged from 0 (no methylation) to 1 (full methylation) of each CpG unit, which contained one or more CpG sites measured as one unit in the MALDI-TOF MS analysis. Aberrant methylation of a CpG unit was defined as when the difference of methylation indexes between two samples exceeded 0.15, which was based on the fact that we have previously found that the differences of *H19*-DMR hypermethylation or *Kv*DMR1 hypomethylation in BWS patients were at least more than 0.15 (data not shown). Since analyzed DMRs included several CpG units, aberrant methylation of a DMR was defined as when more than 60% of total number of analyzed CpG units showed aberrant methylation (with the difference exceeding 0.15). We used CL7 and CBD1 as normal controls in MALDI-TOF MS analysis.

Pyrosequencing

Pyrosequencing was conducted using QIAGEN PyroMark Q24 according to the manufacturer's instruction (Qiagen, Germany). Some of the primers for DMR analysis were described by Woodfine et al. [11]. We designed other primers by using PyroMark Assay Design 2.0 (Qiagen, Germany). The primers for LINE-1 (GenBank accession no. X58075) analyses were described by Bollati et al. [12]. The criterion for MALDI-TOF MS analysis was also employed to define the aberrant methylation of each CpG site and an analyzed region. We used three livers, i.e. CL7, CL16, and CBD1, as normal controls in pyrosequencing. The control livers were analyzed in triplicate for LINE-1 and once for DMRs.

DNA Polymorphism analysis

LOH, UPD, and copy number abnormalities were investigated with DNA polymorphisms. For quantitative analyses, tetranucleotide repeat markers near the imprinted DMRs were amplified and separated by electrophoresis on an Applied Biosystems 3130 genetic analyzer. Data were then quantitatively analyzed with GeneMapper software (Applied Biosystems, CA). The peak height ratios of two parental alleles were calculated. A single nucleotide polymorphism (SNP) of *KCNQ1DN* (*rs229897*) was also analyzed.

All primers used in this study are shown in Additional file 1: Table S1.

Statistical analysis

The methylation statuses of the samples were compared in three pairs: adjacent normal liver tissue (A) and control livers (C), denoted as AxC; tumors (T) and control livers, denoted as TxC; tumors and adjacent normal liver tissue, denoted as TxA. The binomial distribution test was performed to compare aberrant hypomethylation and aberrant hypermethylation within each comparison pair (AxC, TxC, and TxA). The Chi squared test or Fisher's exact test was used for comparison between maternally methylated and paternally methylated DMRs and between gametic and somatic DMRs in aberrant hypomethylation and aberrant hypermethylation cases for each comparison pair. For LINE-1 methylation, a paired *t*-test was used to compare tumor and adjacent normal liver tissue, and an independent *t*-test (Welch's *t*-test) was used for comparing tumor or adjacent normal liver tissue with control liver. A p-value less than 0.05 was considered to be statistically significant. Bonferroni correction was performed when needed.

Results

Clinical information of hepatoblastoma cases

Clinical information of the 12 hepatoblastoma cases analyzed in this study are shown in Table 1. Eleven tumors were sporadic (HB01-HB11), and one was associated with BWS (BWS109). The ratio of males to females was 5:7. The mean age at diagnosis was 25.7 months, ranging from 28 days to 7 years and 11 months. In terms of histological features, 5 cases had combined fetal and embryonal types, 3 cases had mixed epithelial and mesenchymal features with teratoid features, 2 cases were fetal types, and 2 cases were hepatoblastomas (not otherwise specified). Using PRETEXT staging [13], 4 cases were stage II, 5 cases were stage III, and 3 cases were stage IV. Ten of twelve cases were undergoing chemotherapy based on the JPLT-2 protocol, but only two cases (HB05 and HB11) regressed to a lower stage after chemotherapy.

Analyses of aberrant methylation and genetic alterations at imprinted DMRs

We selected 33 regions reported previously as imprinted DMRs in the human genome [11,14] (refer to http://www.geneimprint.com/). Our strategy in this study involved screening the methylation levels of DMRs in tumors, their paired adjacent normal tissues, and normal control livers by MALDI-TOF MS. The samples that showed aberrant methylation were analyzed again by pyrosequencing to confirm the result. These two methods are the most reliable methods of methylation analysis at present [10,15,16]. First, we analyzed the methylation level of these regions in two normal livers, i.e. CL7 and CBD1, by MALDI-TOF MS (Additional file 2: Figure S1). A total

of 20 DMRs showed almost 50% methylation, however, 8 DMRs (*IGF2R*-DMR2, *IGF2*-DMR0, *IGF2*-DMR2, IG-DMR-CG4, IG-DMR-CG6, *TCEB3C*-DMR, *USP29*-DMR, and *NNAT*-DMR) showed mostly full methylation, and 5 DMRs (*TP73*-DMR, *SPTBN1*-DMR, *WT1-AS*-DMR, *DLK1*-DMR, and *GNASXL*-DMR) showed mostly no methylation. It is highly possible that these regions were not differentially methylated in the normal liver, probably due to tissue-specific and/or age-related features of differential methylation, because most of the regions were also analyzed by pyrosequencing and their methylation statuses were confirmed (Additional file 2: Figure S1).

Next, we screened the methylation status of the 33 DMRs in 12 hepatoblastomas and their paired adjacent normal liver tissue by MALDI-TOF MS. We found aberrant methylation in tumors and also in adjacent liver tissue by comparing the methylation between tumors and normal controls (TxC), tumors and adjacent liver tissue (TxA), and adjacent liver tissue and normal controls (AxC). The definition of aberrant methylation is described in the Methods section. After excluding samples harboring chromosomal abnormalities as described later, we confirmed the aberrant methylation using pyrosequencing, except in the case of *H19*-DMR (representative data is shown in Figure 1 and all data in Additional file 3: Figure S2). Additional normal control liver, CL16, was used in pyrosequencing analyses. The methylation status of *H19*-DMR was analyzed by hot-stop combined bisulfite restriction analysis (COBRA) [17] or bisulfite sequencing because of the difficulty in the primer-design for pyrosequencing (Additional file 4: Figure S3).

In order to exclude aberrantly methylated DMRs, as associated with chromosome abnormalities, such as UPD or copy number abnormality, DNA polymorphism analyses using microsatellites and SNPs were performed on all regions showing aberrant methylation in the MALDI-TOF MS analyses. We found seven genetic alterations in four tumors resulting in aberrant methylation: abnormal allelic copy number of 11p13-p15.5 in HB01, 20q11-q13 in HB05, and 19q13 and 20q13 in HB11; LOH of 7q32.2 and 11p15.5 in HB11; and paternal UPD of 11p13-p15.5 in BWS109 (Figure 2). We speculated the allelic imbalance statuses of these loci according to the results of MALDI-TOF MS analysis and DNA polymorphism analysis (Additional file 5: Figure S4). HB01 would harbor more paternal copies than the maternal copies in 11p13-p15.5. An abnormal allelic copy number of 20q11-q13 in HB05 would represent a higher copy number in the maternal allele than the paternal allele. HB11 would have more maternal copies of 19q13 and more paternal

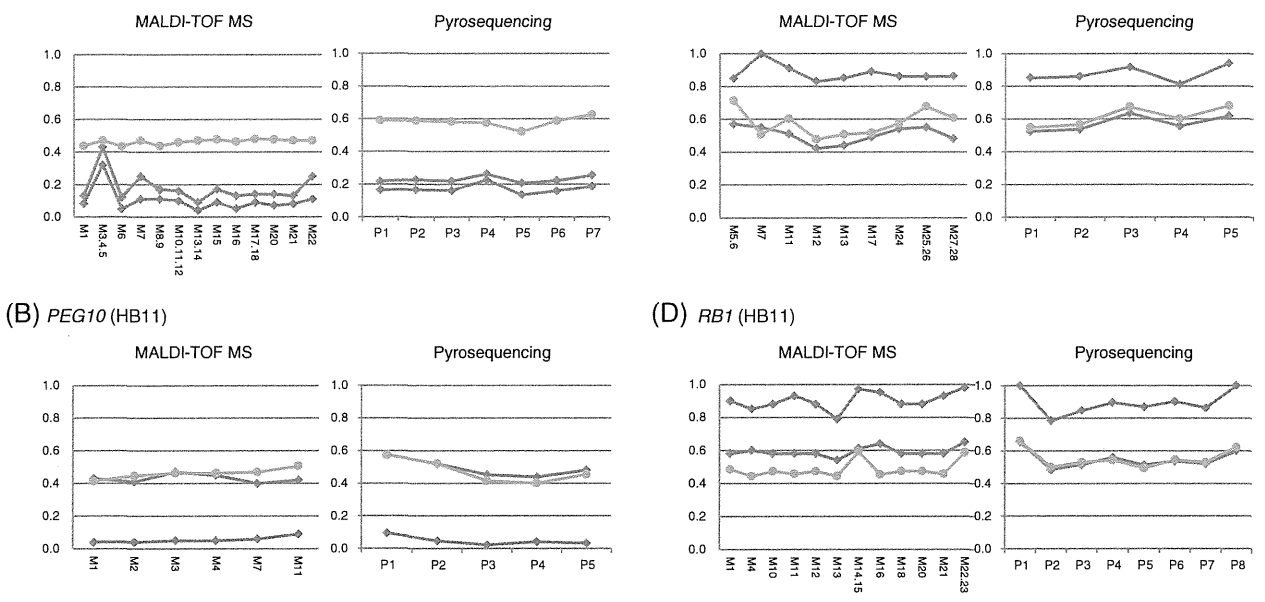

Figure 1 Representative results of methylation analyses by MALDI-TOF MS and pyrosequencing. (A and B) Representative samples of aberrant hypomethylation. *Kv*DMR1 of HB08 and PEG10 of HB11 are shown. *Kv*DMR1 was hypomethylated in both adjacent normal liver and tumor tissues, whereas *PEG10*-DMR was hypomethylated only in tumor tissue. **(C and D)** Representative samples of aberrant hypermethylation. *INPP5Fv2*-DMR in HB05 and *RB1*-DMR in HB11 are shown. Only tumors showed hypermethylation at these DMRs. Aberrant methylation of a DMR was defined as when more than 60% of total CpG units or CpG sites were aberrantly methylated. Aberrant methylation of a CpG unit or CpG site was defined as occurring when the difference of its methylation indexes in two samples exceeded 0.15. The vertical axis represents the methylation index; the horizontal axis represents CpG units (MALDI-TOF MS) or CpG sites (pyrosequencing) analyzed. Green line: average of normal control livers; blue line: adjacent normal liver; red line: tumor (hepatoblastoma).

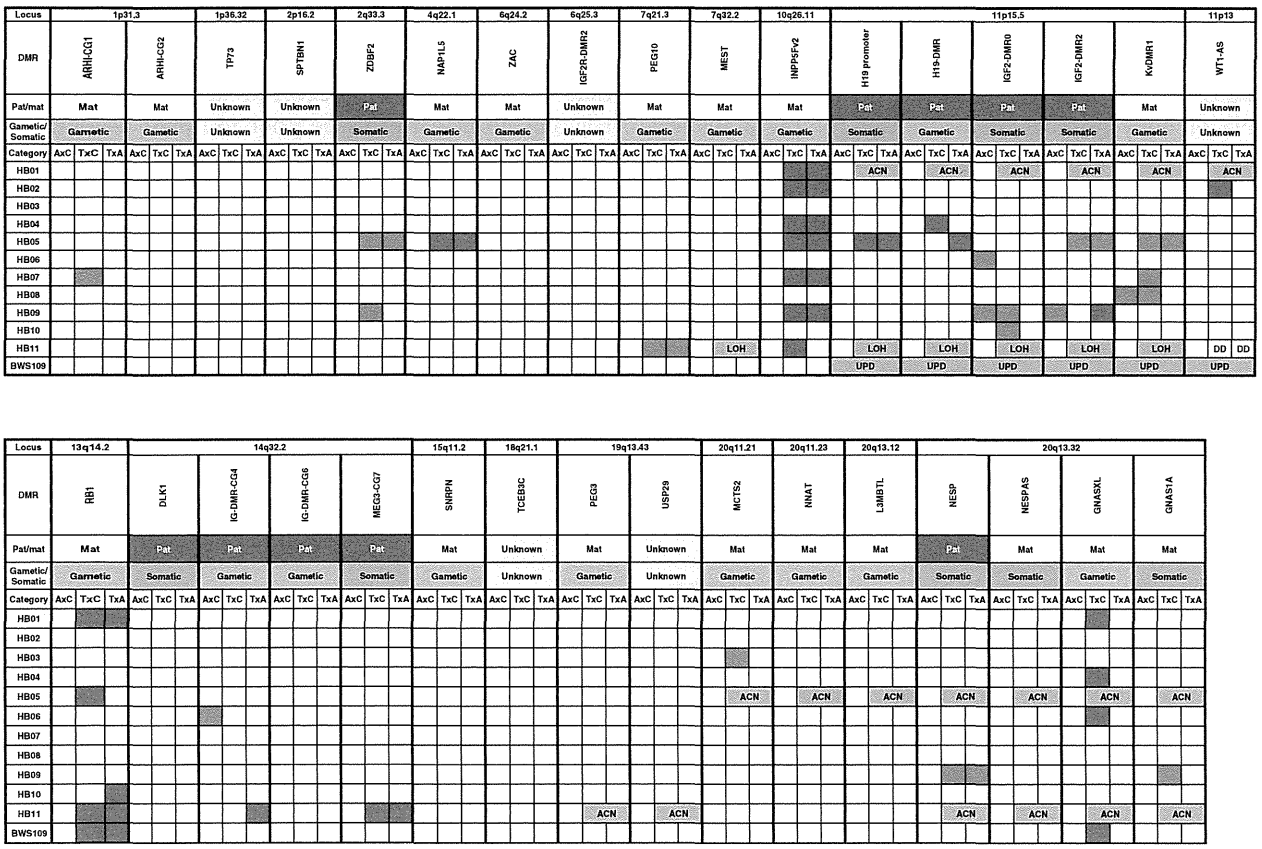

Figure 2 Aberrant methylations and genetic alterations of 33 imprinted DMRs in 12 hepatoblastomas. Aberrant hypomethylation and aberrant hypermethylation found in each comparison are indicated by blue and red boxes, respectively. Aberrant methylation was identified by comparing adjacent normal liver tissue with normal control livers: AxC; tumors compared with normal control livers: TxC; and tumors compared with adjacent normal livers: TxA. The classes of these DMRs in previous reports are shown in Pat/Mat and Gametic/Somatic rows. *ZDBF2*-DMR was tentatively assigned as a somatic DMR based on experiments from mice [35]. MALDI-TOF MS revealed that 13 DMRs, such as *TP73*-DMR, *SPTBN1*-DMR, *IGF2R*-DMR2, *IGF2*-DMR0, *IGF2*-DMR2, *WT1-AS*-DMR, *DLK1*-DMR, IG-DMR-CG4, IG-DMR-CG6, *TCEB3C*-DMR, *USP29*-DMR, *NNAT*-DMR, and *GNASXL*-DMR did not show differential methylation in control livers. Most of these methylation statuses were confirmed by pyrosequencing analysis. Mat: maternally methylated DMR; Pat: paternally methylated DMR; gametic: gametic DMR; somatic: somatic DMR. ACN: abnormal copy number; LOH: loss of heterozygosity; UPD: paternal uniparental disomy; DD: difficult to decide.

copies of 20q13. LOH of 7q32.2 and 11p15.5 would have occurred due to a paternal deletion and a maternal deletion, respectively. The paternal UPD was confirmed using the parents' DNA (Additional file 5: Figure S4). The extent of the UPD was found to be at 11p11.2–pter by a SNP array analysis (data not shown).

The following results described are shown in Figure 2. All tumors carried aberrant methylation in at least one DMR. HB05 carried aberrant methylations at 8 DMRs, the highest number of aberrant methylations, whereas HB03 and HB08 carried aberrant methylations at only one DMR, *MCTS2*-DMR and *Kv*DMR1, respectively. A total of 18 of 33 DMRs showed aberrant methylation, whereas 15 DMRs did not show such features in any tumors. There was large deviation in the incidence of aberrant methylation among the DMRs. *Kv*DMR1 and *IGF2*-DMR0 were the most frequently hypomethylated DMRs in 3 of 9 tumors. The most frequently hypermethylated DMR was *INPP5Fv2*-DMR, which occurred in 7 of 12 samples. *RB1*-DMR was also hypermethylated with a high frequency, which occurred in 5 of 12 samples. In addition, *GNASXL*-DMR was hypermethylated in 4 of 10 samples. The following DMRs showed aberrant methylation in only one tumor: *ARH1*-CG1, *NAP1L5*-DMR, *PEG10*-DMR, *H19* promoter, *WT1-AS*-DMR, *MEG3-CG7*-DMR, *MCTS2*-DMR, *NESP*-DMR, and *GNAS1A*-DMR.

Two chromosomal loci, 11p15.5 and 20q13.32, showed high frequencies of genetic and epigenetic alterations at 10 of 12 and 7 of 12, respectively. In the 11p15.5 locus, seven tumors carried the aberrant methylation and three samples carried genetic alterations. In the 20q13.32 locus, five tumors carried aberrant methylation and two carried an abnormal allelic copy number.

Comparisons of aberrantly methylated DMRs

We compared the numbers of aberrantly hypomethylated and hypermethylated DMRs in three pairs of the sample groups (Figure 3A). We excluded the DMRs harboring UPD or copy number abnormalities for the statistical analyses. Comparing adjacent normal liver tissues (A) and control livers (C), herein denoted as AxC, only hypomethylation was observed in adjacent normal liver tissue ($p = 0.031$). In the TxC comparison, both hypermethylation and hypomethylation were observed in tumors (no significant difference). In the TxA comparison, hypermethylation was observed more frequently than hypomethylation with statistical significance ($p = 0.013$). In addition, the number of hypomethylated DMRs in tumors was higher than that of adjacent normal liver tissue ($p = 0.040$), although Bonferroni correction did not show statistical significance of the difference with a significance level of 0.05/3 (approximately 0.0167). These results suggested a possibility that hypomethylation occurred at certain DMRs in adjacent normal liver tissue prior to tumor development, whereas hypermethylation occurred only within the tumor tissue itself.

We further compared the frequencies of aberrant methylation between paternally methylated DMRs and maternally methylated DMRs. As for hypomethylation, there was no significant difference between the two kinds of DMRs in each comparison (Figure 3B, left panel). In contrast, hypermethylation, which was observed only in tumors, tended to occur more frequently at maternally methylated DMRs than paternally methylated DMRs in the TxC comparison

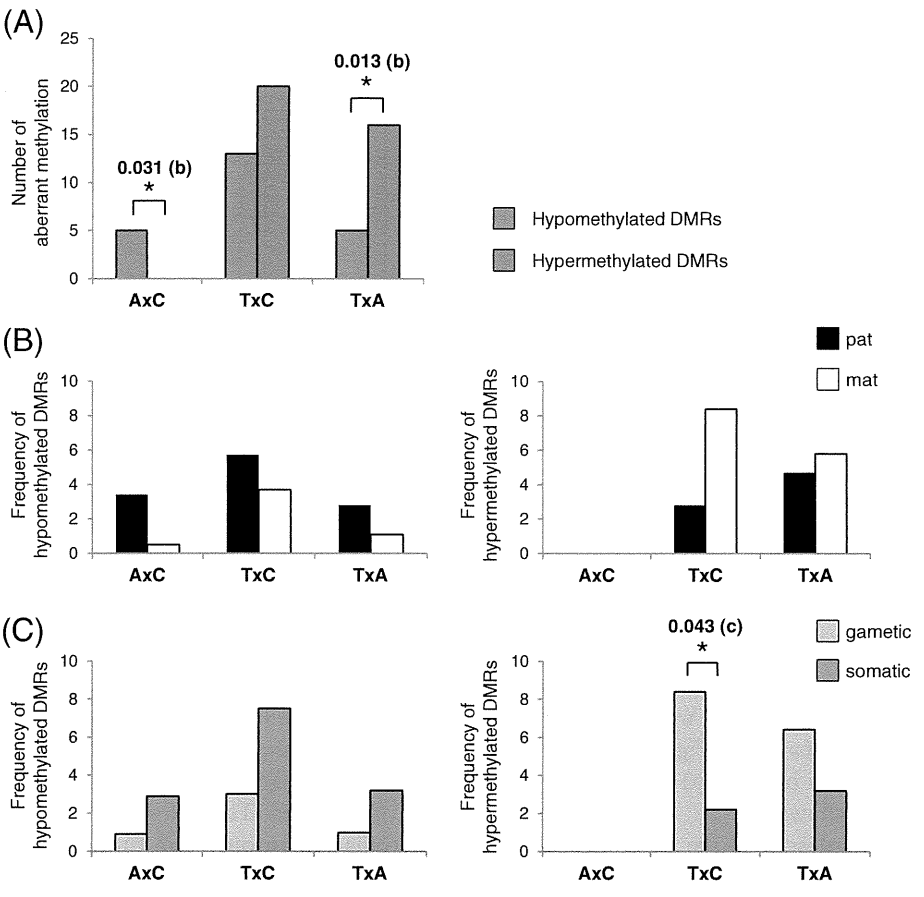

Figure 3 Comparison of aberrant methylations of DMRs in hepatoblastoma. (A) Comparison of the numbers of aberrantly hypomethylated (blue bars) and hypermethylated (red bars) DMRs. Hypomethylation, but not hypermethlation, was observed in adjacent normal tissues. Hypermethylation was observed more frequently than hypomethylation in tumors compared to adjacent normal tissues. **(B)** Comparison of the frequencies of aberrant methylations between the paternally methylated DMRs (black bars) and the maternally methylated DMRs (white bars). Left and right panels indicate hypomethylation and hypermethylation, respectively. There was no significant difference in both hypomethylation and hypermethylation. **(C)** Comparison of the frequencies of aberrant methylations between gametic DMRs (yellow bars) and somatic DMRs (green bars). Left and right panels indicate hypomethylation and hypermethylation, respectively. Hypermethylation was observed more frequently at gametic DMRs with statistically significant difference in tumors compared to control livers. The frequencies were compared in **(B)** and **(C)** because of the difference in the total numbers of DMRs in the two categories compared; that is, the paternal and the maternal DMRs or the gametic and the somatic DMRs. The asterisks indicated significant difference. The p values are shown above the comparisons. b: binomial test, c: chi squared test.

(p = 0.060) (Figure 3B, right panel). We also compared the frequencies of aberrant methylation between gametic DMRs and somatic DMRs. No significant difference in hypomethylation was found between the two kinds of DMRs in each comparison (Figure 3C, left panel). In contrast to hypomethylation, hypermethylation occurred at gametic DMRs more frequently with statistical significance (p = 0.043) (Figure 3C, right panel). This difference was mainly due to the frequent occurrence of hypermethylation at three maternally methylated and gametic DMRs, such as *INPP5Fv2*-DMR, *RB1*-DMR, and *GNASXL*-DMR (Figure 2).

Methylation status of LINE-1 in hepatoblastoma

We analyzed the methylation status of LINE-1 in all samples by pyrosequencing to assess the genome-wide methylation level. LINE-1 is a human repetitive element and constitutes approximately 30% of the human genome [18]. Its methylation status has been used as a surrogate marker for genome-wide DNA hypomethylation in many cancers [19,20]. We analyzed the methylation of four CpG sites in a LINE-1 sequence that were hypomethylated in cancers [21,22]. We compared the methylation levels of each CpG site among the three groups using Bonferroni correction with significance level of 0.0167 (Figure 4). Tumors showed slight hypomethylation only at CpG1 among four CpGs (p = 0.015 in TxA). However, other CpG sites did not show hypomethylation although bare hypermethylations (less than 2.5%) was found only in adjacent normal liver tissues at CpG2 (p = 0.001 in AxC and p = 0.010 in AxT). These results suggested that the genome-wide methylation levels were almost same among three sample groups.

Discussion

In this study, we found many imprinted DMRs methylated aberrantly in hepatoblastomas and paired adjacent normal liver tissue. An important finding was that the aberrant hypomethylation occurred not only in tumor tissue but also in adjacent normal liver tissue. One possible explanation is that the occurrence of the aberrant hypomethylation at certain DMRs may be a very early and specific event prior to tumor development, although there is another possibility that the tumor may induce methylation changes in the adjacent tissues. Okamoto et al. have previously reported a similar phenomenon with respect to aberrant hypermethylation of *H19*-DMR that was frequently found in normal tissues adjacent to Wilms' tumors, which carried the same aberrant methylation [23]. Based on the results, it was hypothesized that the preceding aberrant methylation may be a constitutional aberration in the onset of embryonal tumors. In contrast to the hypomethylation, the aberrant hypermethylation of the DMR occurred only in tumors. These results indicated that the hypermethylation of the DMRs, especially for *INPP5Fv2*-DMR, *RB1*-DMR, and *GNASXL*-DMR, was a specific event for tumor development; this suggested that the pre-cancerous cells did not carry hypermethylation at the DMRs, but acquired the aberrant methylation during tumor development.

We also analyzed the genome-wide methylation level, represented by LINE-1 methylation, and we did not find large difference among three sample groups as a

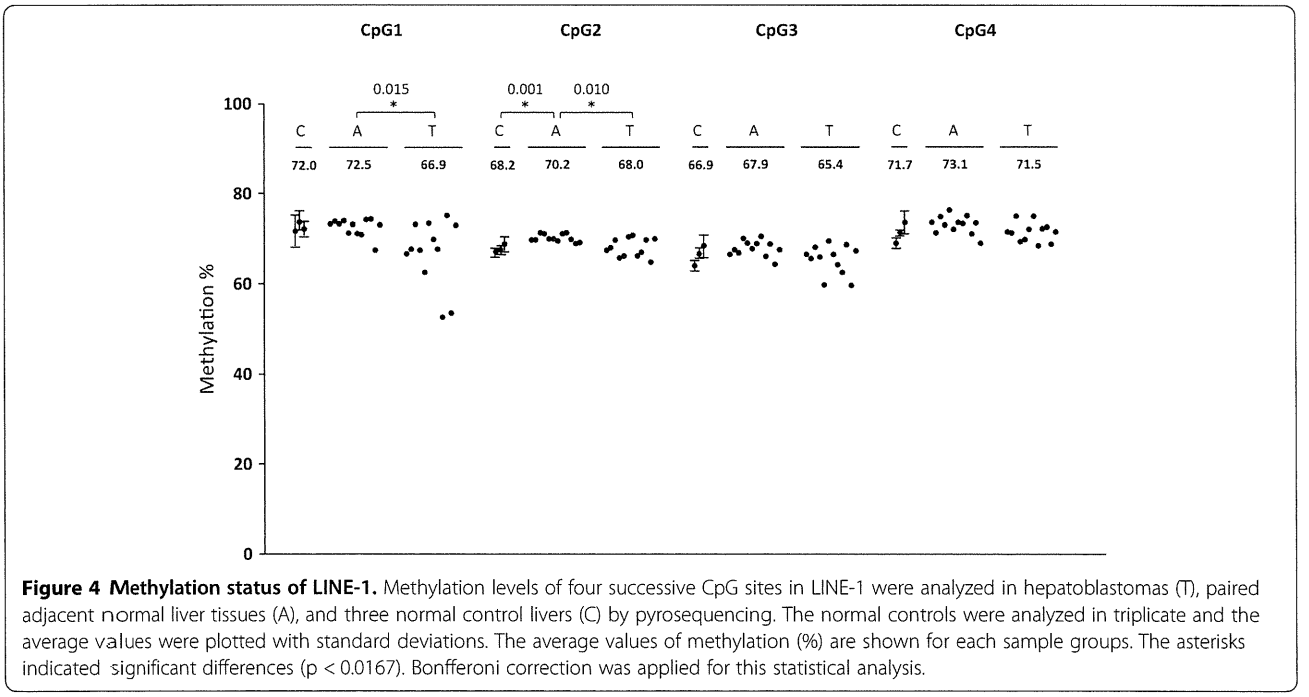

Figure 4 Methylation status of LINE-1. Methylation levels of four successive CpG sites in LINE-1 were analyzed in hepatoblastomas (T), paired adjacent normal liver tissues (A), and three normal control livers (C) by pyrosequencing. The normal controls were analyzed in triplicate and the average values were plotted with standard deviations. The average values of methylation (%) are shown for each sample groups. The asterisks indicated significant differences (p < 0.0167). Bonfferoni correction was applied for this statistical analysis.

whole. LINE-1 is usually hypomethylated in many adult tumors, and its methylation level correlates with clinicopathological features of the tumors [19]. The different situation concerning LINE-1 methylation between hepatoblastoma and adult tumors may reflect a different mechanism of tumorigenesis in embryonal tumors as compared to adult tumors.

Hypermethylation in tumors was frequently observed at three DMRs, *INPPF5v2*-DMR, *RB1*-DMR, and *GNASXL*-DMR. *INPPF5v2*-DMR controls the expression of *INPP5F* transcript variant 2, which encodes a protein of an unknown function [24,25]. *RB1*-DMR, located in intron 2 of the *RB1* gene, leads to maternal expression of transcript variants from exon 2B with very low expression in normal tissues [26]. The function of the variants in cell proliferation is not known. Thus, the effect of these hypermethylated DMRs on tumorigenesis would be little or unknown. *GNASXL*-DMR is associated with the paternal expression of *GNASXL*, which encodes a protein involved in signal transduction [27-29]. The DMR was shown to be mostly unmethylated in control livers (Additional file 2: Figure S1). Thus, hypermethylation of GNASXL-DMR would reduce expression of *GNASXL*. Unfortunately, the expression of genes linked to aberrantly methylated DMRs could not be analyzed due to poor RNA quality, which was probably due to effects of chemotherapy and a limited amount of samples. Therefore, we could not assess the involvement of hypermethylation in tumorigenesis of hepatoblastoma.

Another important finding was the frequent occurrence of both genetic and epigenetic alterations at the two chromosomal loci, 11p15.5 and 20q13.3. The 11p15.5 locus is a well-known imprinted locus responsible for BWS, a tumor-predisposing imprinting disorder. The locus was found to be altered genetically and/or epigenetically in 10 of 12 tumors. Hypermethylation at *H19*-DMR and hypomethylation at *IGF2*-DMR0 associated with biallelic expression of *IGF2* were reported in adult and embryological tumors, including hepatoblastoma [6,7]. Hypermethylation at *H19*-DMR and the *H19* promoter also reduced the expression of *H19* in Wilms' tumor [30,31]. In addition to epigenetic alterations, genetic alterations, such as the amplification of paternal alleles leading to overexpression of *IGF2* and LOH of the maternal allele leading to reduced expression of *H19*, were observed in sporadic Wilms' tumors [32,33]. In this study, in addition to the hypermethylations at *H19*-DMR and the *H19* promoter in two tumors, hypomethylation at *IGF2*-DMR0 occurred in another two adjacent normal liver tissues. Further, abnormal allelic copy number, paternal UPD, and maternal LOH of 11p15.5 were observed. The overexpression of *IGF2* and the reduced expression of *H19* would play an important role in tumorigenesis of hepatoblastoma.

The 20q13.3 locus was also altered genetically and/or epigenetically in 7 of 12 tumors. This locus is responsible for pseudohypoparathyroidism, a condition in which pathogenesis is attributed to the tissue specific imprinting of *Gsα*, for example, which occurs in the proximal renal tubule. On the other hand, an extra copy of chromosome 20 has been known to be the most recurrent cytogenetic alteration in hepatoblastoma [2,34]. We found copy number differences of the alleles in this region, suggesting the existence of non-imprinted oncogenic gene(s) in this region.

Many epigenetic and genetic alterations were found at the loci linked to the 33 imprinted DMRs in 12 hepatoblastomas. However, since sample numbers in this study were small, more hepatoblastoma samples should be analyzed to confirm the present data and to evaluate the precise role of these alterations in tumorigenesis in addition to assessing their usefulness as markers for clinical characteristics, such as stage classification, response to chemotherapy, and prognosis. Also needed are the expression analyses of the genes linked to aberrantly methylated DMRs to assess their role in tumor development, although it is very difficult to obtain hepatoblastoma samples without any chemotherapeutic history.

Conclusions

We found epigenetic and genetic characteristics of hepatoblastoma by comprehensive epigenetic and genetic analyses of 33 DMRs linked to imprinting loci in 12 hepatoblastoma samples and their adjacent normal liver tissues. These included aberrant hypomethylation in adjacent normal liver tissue, tumor-specific hypermethylation, and the frequent occurrence of both genetic and epigenetic alterations at 11p15.5 and 20q13.3 loci. Further studies using more hepatoblastoma samples are needed to confirm the present results and evaluate their roles in the tumor development.

Additional files

Additional file 1: Table S1. Primers used for this study.

Additional file 2: Figure S1. Maps of DMRs analyzed in this study and their methylation status in normal control livers. Upper part; The arrow represents the position and the direction of the transcription start site (TSS). P: promoter; Cen: centromere; Tel: telomere; yellow box (CGI): CpG island; orange boxes (M): CpG sites analyzed by MALDI-TOF MS; green boxes (P): CpG sites analyzed by pyrosequencing. Numbers with diagonal lines indicate CpG units (MALDI-TOF MS) or CpG sites (pyrosequencing), which could not be analyzed. Figures are not drawn to scale. Lower part; Results of MALDI-TOF MS and pyrosequencing are shown. In methylation graphs, the vertical axis represents the methylation index (0: no methylation; 1: full methylation). The horizontal axis represents CpG units or CpG sites. CL7 was analyzed in duplicate by MALDI-TOF MS analysis. Blue and red lines: CL7; green line: CBD1; dark grey line: CL16.

Additional file 3: Figure S2. Methylation data of the aberrantly methylated DMRs in hepatoblastomas. The results of MALDI-TOF MS (left panel) and pyrosequencing (right panel) are shown. The vertical axis represents the methylation index (0–1); the horizontal axis represents

CpG units (MALDI-TOF MS) or CpG sites (pyrosequencing). Green line: average of control livers; blue line: adjacent normal liver; red line: tumor (hepatoblastoma).

Additional file 4: Figure S3. Methylation status of *H19*-DMR as determined by bisulphite cloning sequencing and hot-stop COBRA. (A) Bisulphite sequencing of HB05, which was heterozygous for *rs2071094*. Filled circle: methylated CpG site; open circle: unmethylated CpG site. *rs2071094*: single nucleotide polymorphisms (A/T). CTCF6: CTCF binding site 6. *TaqI*: *TaqI* site used for hot-stop COBRA. (B) Hot-stop COBRA. End-labeled PCR products were obtained by PCR with ^{32}P labeled reverse primer in the final amplification cycle. The PCR products were digested with *TaqI* overnight and then electrophoresed. Band intensities were quantitated using the FLA-7000 fluoro-image analyzer (Fujifilm, Japan). un: unmethylated control DNA; me: fully methylated control DNA.

Additional file 5: Figure S4. Genetic alterations in hepatoblastoma. (A) Map of 11p15-p13 is shown uppermost. Black box: microsatellite marker; white box: DMR analyzed. Tel: telomere; Cen: centromere. Figure is not drawn to scale. Below the map, the representative data of the methylation analyses and microsatellite analyses are shown for three hepatoblastomas. For HB01 tumor, a high paternal copy number was estimated because of the hypermethylation at the paternally methylated *H19*-DMR and the hypomethylation at the maternally methylated *KvDMR1*. LOH in HB11 tumor was indicated by the near loss of one of two alleles. The maternal allele could have been lost because of hypermethylation at *H19*-DMR and hypomethylation at *KvDMR1*. The deviation of the allelic ratio in adjacent normal liver and tumor tissue indicates paternal UPD mosaicism in BWS109, whereas the allelic ratios in the parental blood were approximately 1. The level of mosaicism was higher in tumor than in adjacent normal liver tissue. In tumor samples, the value of the higher peak was divided by that of the lower peak. In adjacent normal liver and parental samples, the ratios were calculated following the pattern in their related tumor. (B) LOH of 7q32 in HB11 tumor was indicated. Because of the hypermethylation at the maternally methylated *MEST*-DMR, the paternal allele would have been lost. (C) Higher maternal copy number of 19q13 were suggested in HB11 tumor, based on the allelic ratio of *D19S589* and the hypermethylation at the maternally methylated *PEG3*-DMR. (D) Allelic copies of 20q11-q13 in HB05 and HB11 tumors were suggested to be abnormal by the allelic ratios of *D20S438* and *D20S158*. Based on the abnormal methylations at the paternally methylated *NESP*-DMR, HB05 tumor would carry more maternal copies than paternal copies of the locus, whereas in HB11 tumor, the paternal allelic copy number would be higher. (PDF 584 kb)

Abbreviations

DMR: Differentially methylated region; LOH: Loss of heterozygosity; UPD: Uniparental disomy; LINE-1: Long interspersed nuclear element-1; ICR: Imprinting control regions; BWS: Beckwith-Wiedemann syndrome; MALDI-TOF MS: Matrix-assisted laser desorption/ionization time-of-flight mass spectrometry; SNP: Single nucleotide polymorphism; COBRA: Combined bisulfite restriction analysis.

Competing interests

The authors declare that they have no competing interests.

Authors' contributions

JMR made significant contributions to the acquisition and analysis of data and also helped in manuscript preparation. TM, KH[1], HY, and KN[1] made contributions to technical supports and data analyses. RS, KM, RH, KK, YO, TS, TT[3], and TT[8] prepared the tissue samples. KN[5] and KH[5] performed technical support and statistical analyses. SA performed HE analyses of tumor samples. HS conceived the study, participated in its design and supervision and prepared the manuscript. KJ also participated in the design and supervision of the study and the preparation of the manuscript. All authors read and approved the final manuscript.

Acknowledgements

We thank Prof. Yutaka Kondo, Division of Epigenomics, Aichi Cancer Center Research Institute, Japan for technical advices in LINE-1 methylation analysis. This study was supported, in part, by a Grant for Research on Intractable Diseases from the Ministry of Health, Labor, and Welfare; a Grant for Child Health and Development from the National Center for Child Health and Development; and, a Grant-in-Aid for Challenging Exploratory Research and a Grant-in-Aid for Young Scientists (B) from the Japan Society for the Promotion of Science.

Author details

[1]Department of Biomolecular Sciences, Division of Molecular Genetics & Epigenetics, Faculty of Medicine, Saga University, Nabeshima 5-1-1, Saga 849-8501, Japan. [2]Faculty of Medicine, Sam Ratulangi University, Manado, Indonesia. [3]Department of Pediatric Surgery, Faculty of Medicine, Kyushu University, Fukuoka, Japan. [4]Department of Pediatrics, Toho University, Omori Medical Center, Tokyo, Japan. [5]Department of Maternal-Fetal Biology, National Research Institute for Child Health and Development, Tokyo, Japan. [6]Department of Pathology and Microbiology, Division of Pathology, Faculty of Medicine, Saga University, Saga, Japan. [7]Department of Anatomic Pathology, Pathological Sciences, Graduate School of Medical Sciences, Kyushu University, Fukuoka, Japan. [8]Department of Pediatric Surgery, Graduate School of Medical Science, Kyoto Prefectural University of Medicine, Kyoto, Japan.

Received: 13 March 2013 Accepted: 20 December 2013
Published: 27 December 2013

References

1. Herzog CE, Andrassy RJ, Eftekhari F: **Childhood cancers: hepatoblastoma.** *Oncologist* 2000, **5**(6):445–453.
2. Tomlinson GE, Kappler R: **Genetics and epigenetics of hepatoblastoma.** *Pediatr Blood Cancer* 2012, **59**(5):785–792.
3. Tomizawa S, Sasaki H: **Genomic imprinting and its relevance to congenital disease, infertility, molar pregnancy and induced pluripotent stem cell.** *J Hum Genet* 2012, **57**(2):84–91.
4. Murrell A: **Genomic imprinting and cancer: from primordial germ cells to somatic cells.** *ScientificWorldJournal* 2006, **6**:1888–1910.
5. Choufani S, Shuman C, Weksberg R: **Beckwith-Wiedemann syndrome.** *Am J Med Genet C: Semin Med Genet* 2010, **154C**(3):343–354.
6. Scelfo RA, Schwienbacher C, Veronese A, Gramantieri L, Bolondi L, Querzoli P, Nenci I, Calin GA, Angioni A, Barbanti-Brodano G, *et al*: **Loss of methylation at chromosome 11p15.5 is common in human adult tumors.** *Oncogene* 2002, **21**(16):2564–2572.
7. Honda S, Arai Y, Haruta M, Sasaki F, Ohira M, Yamaoka H, Horie H, Nakagawara A, Hiyama E, Todo S, *et al*: **Loss of imprinting of IGF2 correlates with hypermethylation of the H19 differentially methylated region in hepatoblastoma.** *Br J Cancer* 2008, **99**(11):1891–1899.
8. Chitragar S, Iyer VK, Agarwala S, Gupta SD, Sharma A, Wari MN: **Loss of heterozygosity on chromosome 11p15.5 and relapse in hepatoblastomas.** *Eur J Pediatr Surg* 2011, **21**(1):50–53.
9. Holm TM, Jackson-Grusby L, Brambrink T, Yamada Y, Rideout WM, Jaenisch R: **Global loss of imprinting leads to widespread tumorigenesis in adult mice.** *Cancer Cell* 2005, **8**(4):275–285.
10. Ehrich M, Nelson MR, Stanssens P, Zabeau M, Liloglou T, Xinarianos G, Cantor CR, Field JK, van den Boom D: **Quantitative high-throughput analysis of DNA methylation patterns by base-specific cleavage and mass spectrometry.** *Proc Natl Acad Sci U S A* 2005, **102**(44):15785–15790.
11. Woodfine K, Huddleston JE, Murrell A: **Quantitative analysis of DNA methylation at all human imprinted regions reveals preservation of epigenetic stability in adult somatic tissue.** *Epigenetics Chromatin* 2011, **4**(1):1.
12. Bollati V, Baccarelli A, Hou L, Bonzini M, Fustinoni S, Cavallo D, Byun HM, Jiang J, Marinelli B, Pesatori AC, *et al*: **Changes in DNA methylation patterns in subjects exposed to low-dose benzene.** *Cancer Res* 2007, **67**(3):876–880.
13. Roebuck DJ, Aronson D, Clapuyt P, Czauderna P, dJe Ville de Goyet J, Gauthier F, Mackinlay G, Maibach R, McHugh K, Olsen OE, *et al*: **2005 PRETEXT: a revised staging system for primary malignant liver tumours of childhood developed by the SIOPEL group.** *Pediatr Radiol* 2007, **37**(2):123–132. quiz 249–150.
14. Higashimoto K, Nakabayashi K, Yatsuki H, Yoshinaga H, Jozaki K, Okada J, Watanabe Y, Aoki A, Shiozaki A, Saito S, *et al*: **Aberrant methylation of H19-DMR acquired after implantation was dissimilar in soma versus placenta of patients with Beckwith-Wiedemann syndrome.** *Am J Med Genet A* 2012, **158A**(7):1670–1675.
15. Tost J, Dunker J, Gut IG: **Analysis and quantification of multiple methylation variable positions in CpG islands by Pyrosequencing.** *Biotechniques* 2003, **35**(1):152–156.

16. Claus R, Wilop S, Hielscher T, Sonnet M, Dahl E, Galm O, Jost E, Plass C: **A systematic comparison of quantitative high-resolution DNA methylation analysis and methylation-specific PCR.** *Epigenetics* 2012, **7**(7):772–780.
17. Uejima H, Lee MP, Cui H, Feinberg AP: **Hot-stop PCR: a simple and general assay for linear quantitation of allele ratios.** *Nat Genet* 2000, **25**(8):375–376.
18. Hancks DC, Kazazian HH: **Active human retrotransposons: variation and disease.** *Curr Opin Genet Dev* 2012, **22**(3):191–203.
19. Takai D, Yagi Y, Habib N, Sugimura T, Ushijima T: **Hypomethylation of LINE1 retrotransposon in human hepatocellular carcinomas, but not in surrounding liver cirrhosis.** *Jpn J Clin Oncol* 2000, **30**(7):306–309.
20. Kitkumthorn N, Mutirangura A: **Long interspersed nuclear element-1 hypomethylation in cancer: biology and clinical applications.** *Clin Epigenetics* 2011, **2**(2):315–330.
21. An B, Kondo Y, Okamoto Y, Shinjo K, Kanemitsu Y, Komori K, Hirai T, Sawaki A, Tajika M, Nakamura T, *et al*: **Characteristic methylation profile in CpG island methylator phenotype-negative distal colorectal cancers.** *Int J Cancer* 2010, **127**(9):2095–2105.
22. Okamoto Y, Sawaki A, Ito S, Nishida T, Takahashi T, Toyota M, Suzuki H, Shinomura Y, Takeuchi I, Shinjo K, *et al*: **Aberrant DNA methylation associated with aggressiveness of gastrointestinal stromal tumour.** *Gut* 2012, **61**(3):392–401.
23. Okamoto K, Morison IM, Taniguchi T, Reeve AE: **Epigenetic changes at the insulin-like growth factor II/H19 locus in developing kidney is an early event in Wilms tumorigenesis.** *Proc Natl Acad Sci U S A* 1997, **94**(10):5367–5371.
24. Choi JD, Underkoffler LA, Wood AJ, Collins JN, Williams PT, Golden JA, Schuster EF, Loomes KM, Oakey RJ: **A novel variant of Inpp5f is imprinted in brain, and its expression is correlated with differential methylation of an internal CpG island.** *Mol Cell Biol* 2005, **25**(13):5514–5522.
25. Monk D, Arnaud P, Frost JM, Wood AJ, Cowley M, Martin-Trujillo A, Guillaumet-Adkins A, Iglesias Platas I, Camprubi C, Bourc'his D, *et al*: **Human imprinted retrogenes exhibit non-canonical imprint chromatin signatures and reside in non-imprinted host genes.** *Nucleic Acids Res* 2011, **39**(11):4577–4586.
26. Kanber D, Berulava T, Ammerpohl O, Mitter D, Richter J, Siebert R, Horsthemke B, Lohmann D, Buiting K: **The human retinoblastoma gene is imprinted.** *PLoS Genet* 2009, **5**(12):e1000790.
27. Hayward BE, Kamiya M, Strain L, Moran V, Campbell R, Hayashizaki Y, Bonthron DT: **The human GNAS1 gene is imprinted and encodes distinct paternally and biallelically expressed G proteins.** *Proc Natl Acad Sci USA* 1998, **95**(17):10038–10043.
28. Pasolli HA, Klemke M, Kehlenbach RH, Wang Y, Huttner WB: **Characterization of the extra-large G protein alpha-subunit XLalphas. I. Tissue distribution and subcellular localization.** *J Biol Chem* 2000, **275**(43):33622–33632.
29. Klemke M, Pasolli HA, Kehlenbach RH, Offermanns S, Schultz G, Huttner WB: **Characterization of the extra-large G protein alpha-subunit XLalphas. II. Signal transduction properties.** *J Biol Chem* 2000, **5**(43):33633–33640.
30. Moulton T, Crenshaw T, Hao Y, Moosikasuwan J, Lin N, Dembitzer F, Hensle T, Weiss L, McMorrow L, Loew T: **Epigenetic lesions at the H19 locus in Wilms' tumour patients.** *Nat Genet* 1994, **7**(3):440–447.
31. Steenman MJ, Rainier S, Dobry CJ, Grundy P, Horon IL, Feinberg AP: **Loss of imprinting of IGF2 is linked to reduced expression and abnormal methylation of H19 in Wilms' tumour.** *Nat Genet* 1994, **7**(3):433–439.
32. Satoh Y, Nakadate H, Nakagawachi T, Higashimoto K, Joh K, Masaki Z, Uozumi J, Kaneko Y, Mukai T, Soejima H: **Genetic and epigenetic alterations on the short arm of chromosome 11 are involved in a majority of sporadic Wilms' tumours.** *Br J Cancer* 2006, **95**(4):541–547.
33. Erson A, Petty E: **Kidney: Nephroblastoma (Wilms tumor).** *Atlas Genet Cytogenet Oncol Haematol* 2007, **11**(1):50–53.
34. Steenman M: **Liver: Hepatoblastoma.** *Atlas Genet Cytogenet Oncol Haematol* 2002, **6**(1):50–52.
35. Kobayashi H, Sakurai T, Sato S, Nakabayashi K, Hata K, Kono T: **Imprinted DNA methylation reprogramming during early mouse embryogenesis at the Gpr1-Zdbf2 locus is linked to long cis-intergenic transcription.** *FEBS Lett* 2012, **586**(6):827–833.

doi:10.1186/1471-2407-13-608
Cite this article as: Rumbajan *et al.*: Comprehensive analyses of imprinted differentially methylated regions reveal epigenetic and genetic characteristics in hepatoblastoma. *BMC Cancer* 2013 **13**:608.

PLOS | GENETICS

Ash1l Methylates Lys36 of Histone H3 Independently of Transcriptional Elongation to Counteract Polycomb Silencing

Hitomi Miyazaki[1,2☯], Ken Higashimoto[1☯], Yukari Yada[3☯], Takaho A. Endo[4¶], Jafar Sharif[4¶], Toshiharu Komori[3,5], Masashi Matsuda[4], Yoko Koseki[4], Manabu Nakayama[6], Hidenobu Soejima[1], Hiroshi Handa[5], Haruhiko Koseki[4,7], Susumu Hirose[3], Kenichi Nishioka[1,2,3]*

1 Division of Molecular Genetics and Epigenetics, Department of Biomolecular Sciences, Faculty of Medicine, Saga University, 5-1-1 Nabeshima, Saga City, Saga, Japan, **2** Precursory Research for Embryonic Science and Technology (PRESTO), Japan Science and Technology Agency (JST), 4-1-8 Honcho, Kawaguchi City, Saitama, Japan, **3** Division of Gene Expression, Department of Developmental Genetics, National Institute of Genetics, 1111 Yata, Mishima City, Shizuoka, Japan, **4** RIKEN Center for Integrative Medical Sciences, RIKEN Yokohama Institute, 1-7-22 Suehiro-cho, Tsurumi-ku, Yokohama City, Kanagawa, Japan, **5** Graduate School of Bioscience and Biotechnology, Tokyo Institute of Technology, 4259 Nagatsuta, Yokohama City, Kanagawa, Japan, **6** Laboratory of Medical Genomics, Department of Human Genome Research, Kazusa DNA Research Institute, 2-6-7 Kazusa-kamatari, Kisarazu City, Chiba, Japan, **7** Core Research for Evolutional Science and Technology (CREST), Japan Science and Technology Agency (JST), 4-1-8 Honcho, Kawaguchi City, Saitama, Japan

Abstract

Molecular mechanisms for the establishment of transcriptional memory are poorly understood. 5,6-dichloro-1-D-ribofuranosyl-benzimidazole (DRB) is a P-TEFb kinase inhibitor that artificially induces the poised RNA polymerase II (RNAPII), thereby manifesting intermediate steps for the establishment of transcriptional activation. Here, using genetics and DRB, we show that mammalian Absent, small, or homeotic discs 1-like (Ash1l), a member of the trithorax group proteins, methylates Lys36 of histone H3 to promote the establishment of Hox gene expression by counteracting Polycomb silencing. Importantly, we found that Ash1l-dependent Lys36 di-, tri-methylation of histone H3 in a coding region and exclusion of Polycomb group proteins occur independently of transcriptional elongation in embryonic stem (ES) cells, although both were previously thought to be consequences of transcription. Genome-wide analyses of histone H3 Lys36 methylation under DRB treatment have suggested that binding of the retinoic acid receptor (RAR) to a certain genomic region promotes trimethylation in the RAR-associated gene independent of its ongoing transcription. Moreover, DRB treatment unveils a parallel response between Lys36 methylation of histone H3 and occupancy of either Tip60 or Mof in a region-dependent manner. We also found that Brg1 is another key player involved in the response. Our results uncover a novel regulatory cascade orchestrated by Ash1l with RAR and provide insights into mechanisms underlying the establishment of the transcriptional activation that counteracts Polycomb silencing.

Citation: Miyazaki H, Higashimoto K, Yada Y, Endo TA, Sharif J, et al. (2013) Ash1l Methylates Lys36 of Histone H3 Independently of Transcriptional Elongation to Counteract Polycomb Silencing. PLoS Genet 9(11): e1003897. doi:10.1371/journal.pgen.1003897

Editor: Giacomo Cavalli, Centre National de la Recherche Scientifique, France

Received March 22, 2012; **Accepted** September 3, 2013; **Published** November 7, 2013

Funding: This work was supported by grants from the Ministry of Education, Culture, Sports, Science, and Technology of Japan (MEXT), by a Grant for Research on Intractable Diseases from the Ministry of Health, Labor, and Welfare, by funds from Saga University, and by the JST PRESTO program. The funders had no role in study design, data collection and analysis, decision to publish, or preparation of the manuscript.

Competing Interests: The authors have declared that no competing interests exist.

* E-mail: nshoka@cc.saga-u.ac.jp

☯ These authors contributed equally to this work.

¶ TAE and JS also contributed equally to this work.

Introduction

Studies on the regulation of transcriptional memory are challenging. Conceptually, the regulation consists of two phases: establishment and maintenance. Molecular mechanisms for the maintenance of the memory are relatively well understood compared with those for the establishment of memory. Indeed, how the establishment of transcriptional activation occurs is largely unknown because it has been difficult to distinguish mechanisms for establishment from those for maintenance, presumably due to functional redundancies and spatial and temporal overlap between them. Moreover, if transient regulation is involved during the establishment phase, it is extremely difficult to tease apart and analyze the respective underlying mechanisms.

For the establishment of transcriptional activation of developmentally regulated genes in stem cells, we know that the poised RNAPII should be released from pausing in the promoter-proximal coding region, as occurs in response to various microenvironmental cues [1], and that the associated chromatin should be kept competent for transcription by RNAPII throughout a coding region. P-TEFb, a cyclin-dependent kinase complex, plays a pivotal role in the RNAPII pause release by alleviating the repressive effects of DRB sensitivity-inducing factor (DSIF) and negative elongation factor (NELF), and by phosphorylating the Ser2 residue of the carboxyl-terminal domain of RNAPII [2–5]. In

Author Summary

Transcriptional mechanisms in eukaryotes are composed of numerous consecutive steps, including chromatin modification and remodeling. Recent reports using yeast genetics have revealed that Lys36 methylation of histone H3, a hallmark of the active gene, is a consequence of transcriptional elongation. Similarly, a report using *Drosophila* genetics showed that exclusion of the Polycomb repressive complexes, general repressor complexes that regulate development and cellular differentiation, is another consequence of transcription. Here, we provide evidence that these causal relationships are not really general. By ceasing ongoing transcription at a certain step using an inhibitor in combination with mouse genetics, we have identified novel intermediate steps of transcription: Ash1l-mediated Lys36 methylation of histone H3 and subsequent exclusion of the Polycomb complexes that occur independently of transcriptional elongation. Furthermore, we show that binding of a nuclear receptor may promote trimethylation of Lys36 in its associated gene independent of its ongoing transcription. In this paper, we detail previously unknown key machineries orchestrated against Polycomb silencing, providing an innovative view of the mechanisms involved in the establishment of transcriptional memory.

addition to recruitment of P-TEFb, it has been proposed that recruitment of a certain chromatin remodeling factor is also crucial to the release of paused RNAPII [3], which appears to be situated adjacent to the first nucleosome downstream of the transcription start site [6]. Thus, it seems that at least two independent mechanisms are required to trigger productive transcriptional elongation. It is conceivable that these mechanisms are engaged throughout the coding region to maintain active gene expression. In addition, the activation of Polycomb group-target genes further requires several counteracting mechanisms against the Polycomb repressive complexes (PRCs) [7]. However, these mechanisms underlying the establishment of transcriptional memory and how these mechanisms are orchestrated remain elusive.

Ash1l is the mammalian equivalent of the *Drosophila* Ash1 protein. Although Ash1 is one of the first identified members of the trithorax group proteins [7], both the Ash1- and Ash1l-containing complexes remain uncharacterized. Both Ash1 and Ash1l are localized in chromatin and have been identified specifically in promoter-proximal coding regions of a number of active genes [8,9], suggesting a role during an early step of transcriptional elongation. Additionally, artificial tethering of Ash1 to chromatin containing a reporter gene results in gene activation in a SET domain-dependent manner [10]. These results suggest that Ash1 is an epigenetic activator found in an "ON" state of target genes, although the underlying mechanism of its action remains unknown.

Like a number of SET domain-containing proteins, both Ash1 and Ash1l possess histone lysine methyltransferase activity. However, it is currently controversial as to which lysine residue is targeted *in vivo*, although recent reports have suggested that Lys4 and Lys36 of histone H3 are the most plausible candidates [8–11]. So far, Lys4 is widely believed as a target residue due to several lines of *in vivo* evidence [8–10], compared with only one for Lys36 [12]. It is consistent with the activator function of Ash1 [10], while Lys36 methylation (Lys36me) has been shown to occur as a consequence of transcription [13–15]. However, it should be noted that an analysis of the enzymatic activities of Ash1 and Ash1l *in vivo* has been difficult due to their physical and functional interactions with other enzymes that methylate Lys4 [16,17] and also due to the redundancy of enzymes methylating Lys36, such as Setd2, Nsd1, Nsd2 and Nsd3 in mammals. Moreover, expression of the full-length recombinant Ash1l and detection of the endogenous Ash1l by immunoblot has been as yet unsuccessful, thereby making analyses more challenging.

To elucidate the molecular mechanism of the Ash1l-mediated establishment of gene expression, we developed a knock-in allele expressing mutant of Ash1l without part of the SET domain. Using the mutant ES cells, we show that Ash1l methylates Lys36 of histone H3 both *in vitro* and *in vivo*. Importantly, using DRB, a P-TEFb kinase inhibitor that blocks productive transcriptional elongation, we show that the methylation by Ash1l and its effect on PRC exclusion occur independently of productive transcriptional elongation. In particular, an accumulation of Lys36me3 in RAR-associated genes independent of transcriptional elongation implicates a certain special function for establishing transcriptional activation of Polycomb group-target genes. Moreover, the broad chromatin domains carrying Lys36me were co-regulated with the Tip60 or Mof complexes in a region-dependent manner, which in turn acetylate the Lys16 of histone H4. We further investigated a mechanism for the promotion of gene expression by Ash1l, and found an Ash1l-dependent association with Brg1, another founding member of the trithorax group proteins. These molecular data in ES cells are supported by expression patterns of Hox genes and skeletal phenotypes in Ash1l mutant mice. Thus, through genetic and biochemical analyses of Ash1l, we have elucidated a novel cascade of interplays from Ash1l to Brg1, which ultimately promotes chromatin reprogramming that counteracts Polycomb silencing.

Results

Ash1l knock-in mutant ES cells demonstrate impaired retinoic acid response

To explore a function of the methyltransferase activity of mammalian Ash1l, we generated knock-in mice and ES cells expressing mutant Ash1l containing a short in-frame deletion within the AWS-SET domain (represented by ΔSET, Figure 1A). Mouse *Ash1l* mRNA was ubiquitously expressed in embryos, while it was relatively enriched in the adult brain (Figures S1A, S1B and data not shown). Expression of *Ash1l* mRNA was not affected in ΔSET embryos and ES cells (Figures 1B and 1C). Homozygotes were viable and fertile (Table S1).

Since Ash1l is a member of the trithorax group proteins that regulate transcriptional activation of Hox genes, and retinoic acid (RA) is known to induce expression of Hox genes in ES cells, a role for Ash1l methyltransferase activity in RA-induced Hox gene expression was investigated in differentiating ES cells. A culture protocol is shown in Figure 1D. Here, we analyzed representative RA-responsive Hox genes, *Hoxb4*, and *Hoxd4*. Using a series of RA concentrations, we found that expression levels of *Hoxb4* and *Hoxd4* mRNAs were reduced in ΔSET ES cells (Figure 1E). Specifically, the threshold concentration of RA required to trigger the *Hoxd4* mRNA expression was significantly increased in ΔSET ES cells compared with that in wild-type cells (Figure 1F). Moreover, the activation of the *Hoxd4* mRNA expression was relatively slow in ΔSET ES cells (Figure 1G). These results indicate that the methyltransferase activity of Ash1l is necessary for an appropriate response to RA.

We further performed gene expression analyses of RA-treated differentiating ES cells by RNA-sequencing (RNA-Seq) to determine if RA-responsive genes were generally affected in

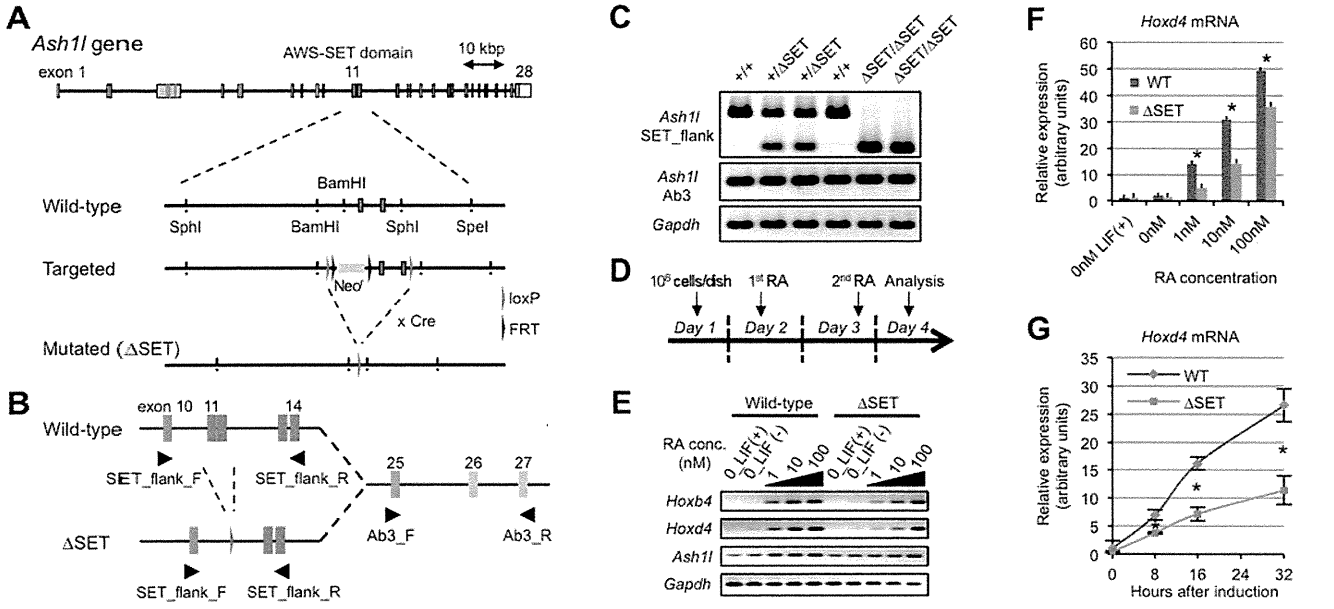

Figure 1. Basic characterization of Ash1l mutant ES cells and Hox gene expression in response to RA. (**A**) Schematic representation of the strategy used for targeted disruption of the *Ash1l* gene. Exons 11–12 encoding the AWS-SET domain with their flanking introns were floxed by loxP sequences. Cre-mediated germ-line recombination resulted in the generation of the ΔSET allele. (**B**) A PCR primer-pair of SET_flank_F/R was used to distinguish between expression from the wild-type allele and that from the ΔSET allele as shown in (A). A PCR primer-pair of Ab3_F/R was used to determine total expression from both alleles. The PCR primer-pairs are listed with their sequences in Table S4. (**C**) Comparison of *Ash1l* mRNA expression among E10.5-litter-mate embryos by conventional RT-PCR. Expression levels of *Gapdh* mRNA are shown as controls. (**D**) Protocol for RA-induced differentiation of ES cells. (**E**) Conventional RT-PCR analyses of *Hoxb4* and *Hoxd4* mRNA expression levels in response to various concentrations of RA. (**F** and **G**) Quantitative RT-PCR analysis of *Hoxd4* mRNA expression levels. RA-titration analysis after 48 hours of induction (F), and a time-course analysis using 1 nM RA (G). The results are represented as relative expression levels between wild-type and ΔSET ES cells. Wild-type cells (blue bars or line) and homozygous ΔSET ES cells (orange bars or line) are shown. These results represent means and standard deviations (s.d.) of three independent PCR reactions (Student's t-test, *$P<0.05$).
doi:10.1371/journal.pgen.1003897.g001

ΔSET ES cells. Among 14,255 annotated genes, there were 543 genes that were highly up-regulated by RA treatment (more than 5-fold). Among those 543 genes, we found 152 genes (28.0%) in ΔSET ES cells showing impaired responses to RA (more than 2-fold decrease compared with wild-type cells, Figure 2A and Table S2), in which several Wnt and Hox family genes appeared to be affected (Figure S2). As expected, gene ontology analysis of the 152 genes revealed that biological functions of Ash1l were highly related to body pattern formation during development (Figure 2B).

The status of chromatin signatures in ES cells can be classified in terms of the presence of Lys4me3 or Lys27me3 in histone H3 polypeptides: Lys4me alone, Bivalent (positive for both Lys4me3 and Lys27me3), Lys27me alone and None (negative for both Lys4me3 and Lys27me3) [18]. Interestingly, the 152 RA-responsive and ΔSET-impaired genes were significantly enriched in a group positive for Lys27me3 (Figure 2C) and further enriched especially in the Bivalent gene group (Figure 2D), suggesting that the methyltransferase activity of Ash1l counteracts Polycomb silencing upon activation of developmentally regulated genes. Chromatin immunoprecipitation-sequencing (ChIP-Seq) analysis revealed that Ash1l was present in more than 30% of those affected genes (Figure 2E).

RNA-Seq analysis of undifferentiated ES cells showed that expression levels of a majority of marker genes, including core stem cell markers, were unchanged, while some endoderm markers were moderately up-regulated in ΔSET ES cells (Figure S3A). RA treatment of ES cells further enhanced the up-regulation (Figure S3B). Comprehensive analysis of RNA expression levels of 14,255 annotated genes revealed that 57 genes were down-regulated more than 2-fold in undifferentiated ΔSET ES cells, while 59 genes were up-regulated (Table S3). Several microRNAs and *Snord* family genes were highly dys-regulated in ΔSET ES cells, although the impact of the methyltransferase activity of Ash1l on these genes *in vivo* remains unclear. While this manuscript was under preparation, a report describing the methyltransferase activity of Ash1l for Hox gene repression was published online [19]. Reason for discrepancy between our results and theirs is currently unknown. However, conditions of basic materials and methods may affect each result: knock-in mutant ES cells and mice for ours, exogenous transient over-expression in K562 cells for theirs.

Ash1l methylates Lys36 of histone H3 *in vitro*

To elucidate an underlying mechanism involved in the regulation of gene expression by Ash1l, we examined the biochemical activity of Ash1l *in vitro*. We employed a bacterially expressed GST-fusion Ash1l protein (Figure 3A) since it has no associated protein that methylates histone polypeptides. As shown in Figure 3B, wild-type Ash1l (NF-WT) methylated histone H3 in nucleosomes, but did not methylate free histone octamers or $(H3\text{-}H4)_2$ tetramers bound to DNA. Addition of H2A-H2B dimers to the $(H3\text{-}H4)_2$ tetramers on DNA in the reaction mixture failed to replicate the methylation activity [K.N. unpublished observation], and an amino acid substitution within the core catalytic part of the SET domain (NF-H2213K) abolished it. Additionally, wild-type Ash1l methylated wild-type histone H3 and its Lys4-to-Ala (K4A) mutant to a similar extent, but not its Lys36-to-Ala (K36A) mutant (Figure 3C). These results clearly indicate that Ash1l specifically

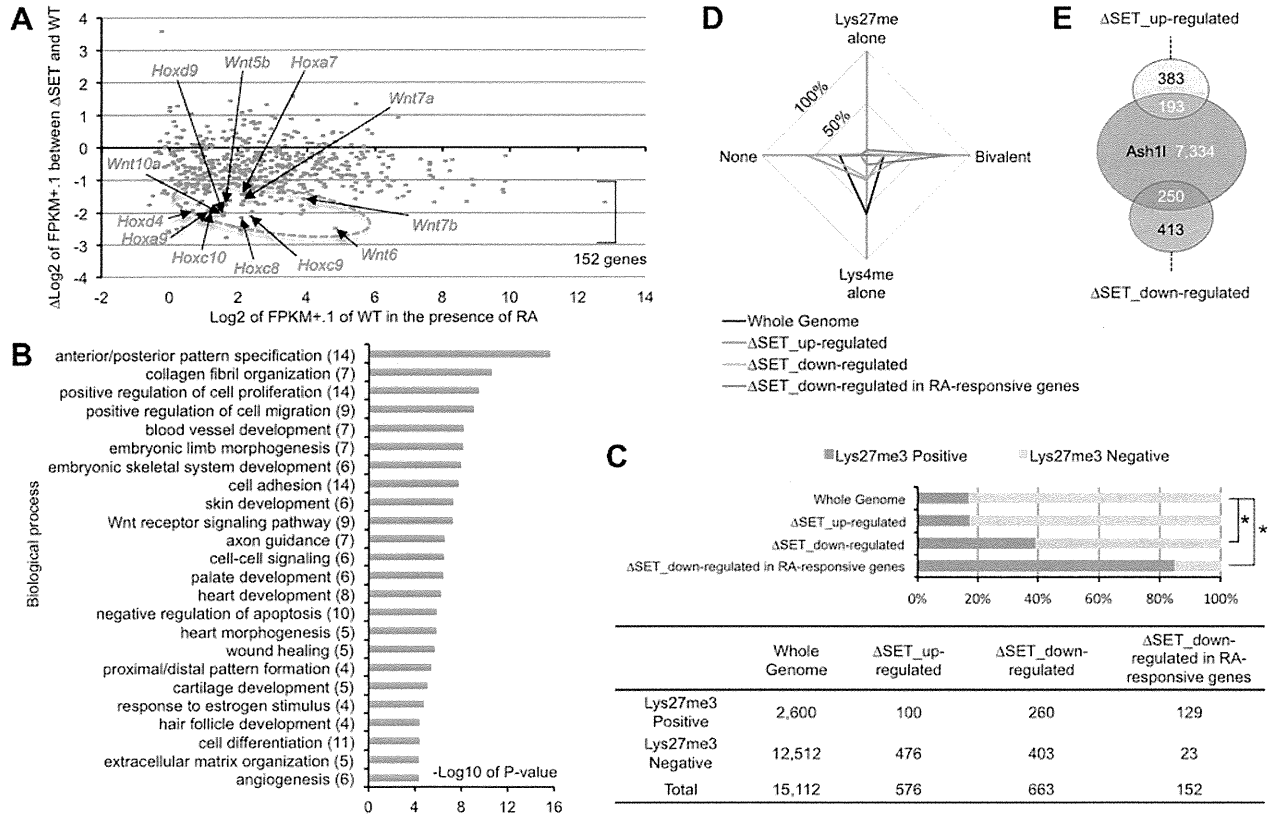

	Whole Genome	ΔSET_up-regulated	ΔSET_down-regulated	ΔSET_down-regulated in RA-responsive genes
Lys27me3 Positive	2,600	100	260	129
Lys27me3 Negative	12,512	476	403	23
Total	15,112	576	663	152

Figure 2. Comprehensive gene expression analyses of differentiating ES cells. ES cells were treated with 10 nM RA for 2 days, and purified total RNA samples were subjected to RNA-Seq analyses. (**A**) RA-responsive genes (those whose expression levels were increased more than 5-fold compared with undifferentiated ES cells: 543 genes out of 14,255 eligible annotated genes) were plotted on the graph using modified fragments/kb of transcript/million fragments mapped (FPKM) values. The x-axis corresponds to expression levels of each gene (shown as log2 transformation of each FPKM value plus 0.1), and the y-axis corresponds to fold change in gene expression levels between ΔSET ES cells and wild-type (shown as Δlog2 transformation). The encircled area was enriched for some Hox and Wnt family genes (arrows, see also Figure S2). (**B**) Gene ontology analysis of ΔSET-impaired 152 genes. A subset of RA-responsive genes demonstrating a greater-than-2-fold decrease in the modified FPKM values in differentiating ΔSET ES cells was analyzed. Gene enrichment P-values were calculated by Chi-square test. The numbers of genes in each group are shown in parentheses. (**C**) Bar chart showing relative ratios of the numbers of genes carrying trimethylation of Lys27 [18], a hallmark of the Polycomb-regulated genes. Genes showing a difference greater than 2-fold were analyzed (up- or down-regulated). In addition, RA-responsive genes in the down-regulated genes were further extracted and analyzed [the last group, same as in (B)]. Chi-square testing was used for calculation of P-values against the total gene set, *$P<0.001$. The numbers of genes in each group are shown in the table below. (**D**) Radar chart showing relative ratio of status of chromatin signatures for indicated gene group as in (C). (**E**) Venn diagram showing the relationship between Ash1l-target genes and ΔSET-affected genes. The numbers of genes in each compartment are shown. The total number of annotated genes analyzed was 18,724.
doi:10.1371/journal.pgen.1003897.g002

methylates Lys36 of histone H3 and presumably recognizes the preinstalled H2A-H2B dimer in a nucleosome to target Lys36. Furthermore, recombinant Ash1l carrying a deletion at the N-terminal flanking region of the AWS domain (ΔNF-WT) was catalytically inactive, indicating that this region is necessary for optimum methyltransferase activity.

Ash1l methylates Lys36 of histone H3 upon gene activation

We next examined whether our *in vitro* results could be recapitulated in an *in vivo* setting. Histone modification patterns and Ash1l occupancy in *Hoxd4* in differentiating ES cells were analyzed by ChIP assays. PCR primer-pairs were set as shown in Figure 3D (Table S4 for sequences). A promoter-proximal coding region of *Gapdh* was also investigated as a constitutively active control. *Hoxd4* chromatin has been reported to be bivalent in undifferentiated ES cells [18]. Consistent with the report, even in the absence of RA, peaks of histone H3 Lys4me2 and me3 (Lys4me2/3) were clearly detected in a promoter-proximal coding region of *Hoxd4*, while the levels of histone H3 Lys36me2 and me3 (Lys36me2/3) were rudimentary (Figure 3E). Surprisingly, Ash1l was clearly present in *Hoxd4* even in the absence of RA (Figure 3E). We also observed considerable amounts of Ash1l in the promoter-proximal coding region of *Gapdh*. However, we observed no difference between wild-type and ΔSET ES cells in these ChIP assays.

Following RA treatment, while the levels of Lys36me2/3 were increased in *Hoxd4* coding regions in wild-type cells, this was not observed in ΔSET ES cells (Figure 3F). There was no significant change in the levels of Lys4me2/3 of *Hoxd4* in ΔSET ES cells. We found that the levels of Ash1l in coding regions of *Hoxd4* and *Gapdh* were maintained after RA treatment. We observed no difference in the levels of Ash1l between wild-type and ΔSET ES cells. These results indicate that Ash1l specifically methylates Lys36 *in vivo*, as expected from our *in vitro* results, and suggest that the enzymatic activity of Ash1l is activated upon the addition of RA. Since Ash1l is a dimethylase [11], the observation that there was no increased Lys36me3 in ΔSET ES cells may be a consequence of an impaired

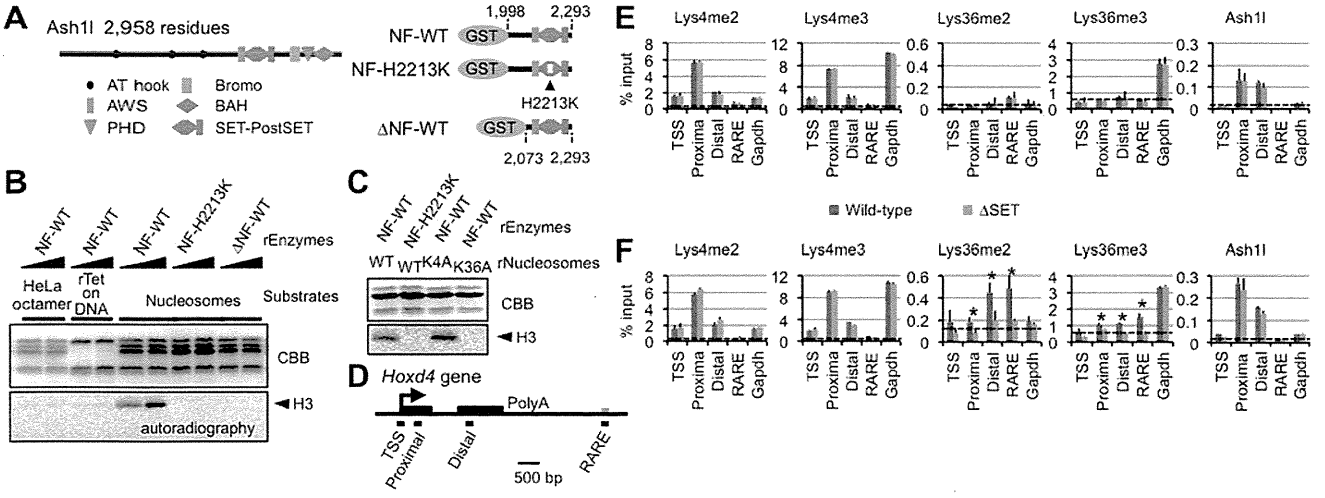

Figure 3. Ash1l specifically methylates Lys36 of histone H3 both *in vitro* and *in vivo*. (**A**) Structure of full-length Ash1l (left) and GST-fusion Ash1l constructs (right). NF: the N-terminal flanking region of the AWS domain, H2213K: amino acid substitution of His2213 to Lys. (**B** and **C**) Histone methyltransferase assays with GST-fusion Ash1l (rEnzyme). rTet on DNA: recombinant $(H3–H4)_2$ tetramers bound to plasmid DNA. rNucleosomes: recombinant nucleosomes containing wild-type or mutant histone H3 as indicated. CBB: Coomassie brilliant blue staining for histone polypeptides separated on a SDS-PAGE gel. Position of histone H3 in the autoradiogram is indicated in each assay (arrowheads). (**D**) Diagram of the *Hoxd4* gene. Black and grey boxes represent exons and a 3′ retinoic acid responsive element (RARE), respectively. Black bars under the diagram indicate the regions analyzed by ChIP assays. TSS: transcription start site. (**E** and **F**) ChIP assays of various regions in differentiating ES cells before (E) or after (F) RA treatment (see the culture protocol shown in Figure 1D). The results are represented as mean values relative to input (% input). Error bars represent s.d. (Student's t-test, *$P<0.05$). The antibodies used are indicated above each graph. Broken lines indicate approximate levels of ChIP signals in the *Il2ra* promoter as a control.
doi:10.1371/journal.pgen.1003897.g003

Lys36me2-platform that is required as a substrate for a certain trimethylase.

Lys36me occurs independently of RNAPII Ser2p

Based on several studies conducted in yeast, the presence of Lys36me in a coding region is widely believed to be a consequence of transcriptional elongation [13–15] and to function to recruit the histone deacetylase complex [20,21]. However, our results suggested a novel hypothesis: Lys36me by Ash1l in a coding region occurs during the establishment of Hox gene activation to promote a proper response to RA (see Figures 1F and 1G). Therefore, in this case, the Lys36me should be independent of the productive transcriptional elongation.

To test our hypothesis, we employed DRB, which reversibly blocks productive transcriptional elongation by inhibiting the kinase activity of P-TEFb. DRB artificially creates the poised RNAPII, closely mimicking the promoter-proximally paused RNAPII in a gene demonstrating bivalent chromatin in ES cells, thereby manifesting intermediate steps for the establishment of transcriptional activation. If Lys36me by Ash1l is independent of the RNAPII Ser2p or transcriptional elongation, then DRB would not affect methylation levels. In the next experiments, DRB was added to differentiating ES cells during RA treatment and ChIP assays were performed. Two Ash1l-associated genes were compared: *Hoxd4*, representing a Polycomb group-target gene, and *Gapdh*, a constitutively active gene.

As shown in Figure 4A, far from a decrease in the Lys36me level, wild-type ES cells displayed a clear increase in Lys36me2/3 levels in the promoter-proximal coding region of *Hoxd4* in response to DRB. Interestingly, differences in the Lys36me2/3 levels between wild-type and ΔSET ES cells were more evident in the presence of DRB. On the other hand, DRB also increased the Lys36me2/3 levels in ΔSET ES cells, albeit to a lesser extent [compare (−) and (+) in ΔSET], suggesting that some Lys36-methylases other than Ash1l could be involved, although the identity of the enzyme recruited to the region has yet to be determined. In *Gapdh*, DRB increased Lys36me2 levels in wild-type cells, but DRB treatment resulted in a clear decrease in Lys36me3 levels (Figure 4B), suggesting that DRB specifically affected association of a certain trimethylase that was recruited in a RNAPII Ser2p-dependent manner. Similar results were obtained for *Hoxb4* and *Hprt1* (Figure S4). These results indicate that Lys36me2 by Ash1l and other dimethylases occurs independently of RNAPII Ser2p. However, whether Lys36me3 occurs independently of RNAPII Ser2p is gene-dependent.

Lys36me2 in a large number of regions occurs independently of the Ser2-phosphorylation of RNAPII, while Lys36me3 occurs in a context-dependent manner

Having established that *Hoxd4* and *Gapdh* were DRB-responsive genes in that Lys36me2(/3) was increased in response to DRB, we analyzed if the observed response was applicable genome-wide. First, immunoblot analyses for bulk Lys36me2 and Lys36me3 levels were performed (Figure 4C). In the presence of RA, we found the bulk Lys36me2 levels in wild-type and ΔSET ES cells were similarly increased in response to DRB, while those of Lys36me3 were not, and instead decreased.

Next, we performed ChIP-Seq analyses to obtain genome-wide profiles of Lys36me2/3 in response to DRB. Distributions of Lys36me2/3 relative to a metagene show a clear difference between Lys36me2 and me3 in response to DRB: Lys36me3 levels were decreased in isolated, entire regions, while in contrast, Lys36me2 levels were increased in most of the regions (Figure 4D). Thus, having observed that Lys36me3 of *Hoxd4* was increased in response to DRB, here we found that its genome-wide level showed the opposite response, indicating that genes demonstrating increased Lys36me3 levels in response to DRB were minorities.

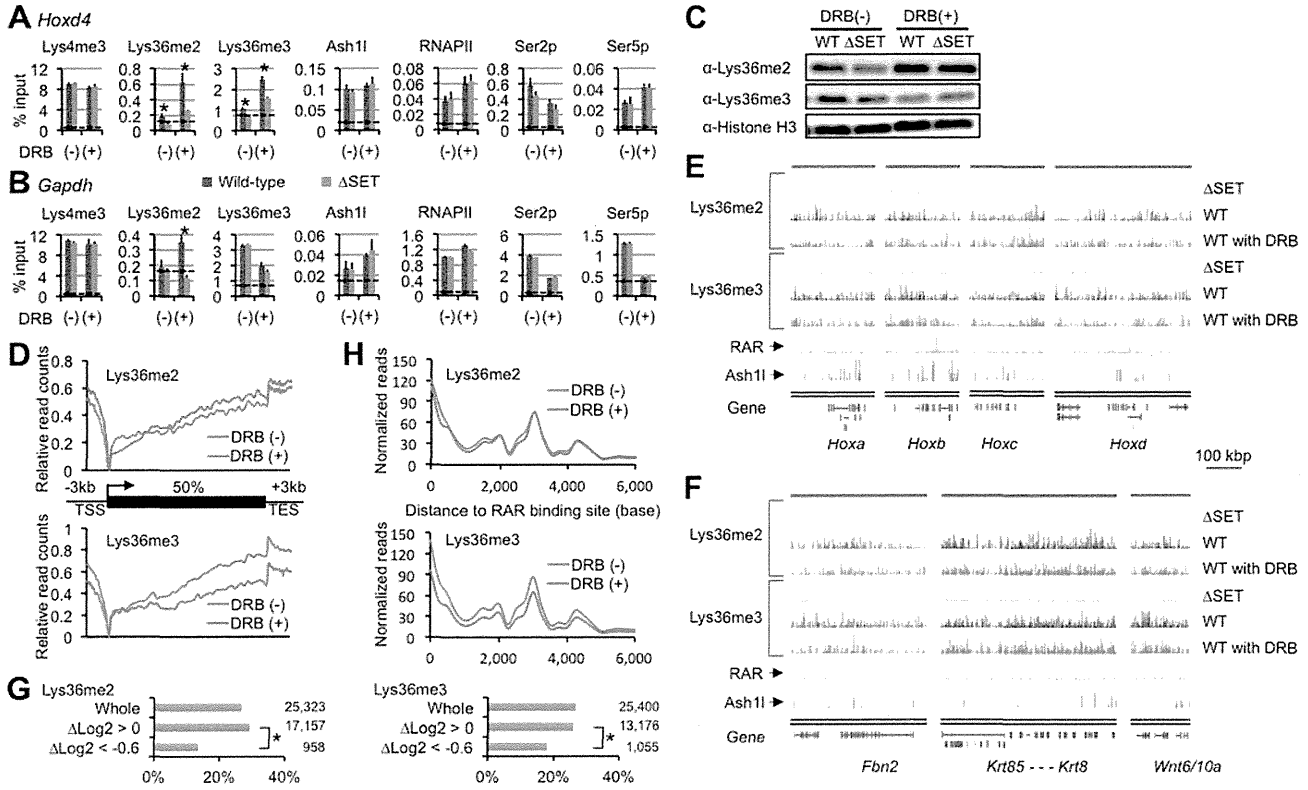

Figure 4. Lys36me2 occurs independently of the Ser2-phosphorylation of RNAPII, while Lys36me3 occurs in a context-dependent manner. ChIP assays of differentiating ES cells either with (+) or without (−) DRB treatment. Promoter-proximal coding regions of either *Hoxd4* (**A**) or *Gapdh* (**B**) were analyzed. DRB was added during RA treatment, and then ES cells were cultured for another 16 hours. The antibodies used are indicated above each graph. The results are represented as means and s.d. (Student's t-test, *P<0.05). Broken lines indicate approximate levels of ChIP signals in either *Il2ra* promoter as controls. (**C**) In the presence or absence of DRB, bulk histones in differentiating ES cells were analyzed by immunoblot using the indicated antibodies. (**D**) Distributions of Lys36me2/3 ChIP-Seq read counts relative to a metagene in the presence or absence of DRB. The y-axis corresponds to relative read counts to base-read counts (shown as log2 transformation). TSS: transcription start site, TES: transcription end site. (**E** and **F**) Genomic profiles for Lys36me2/3, RAR, and Ash1l ChIP-Seq signals of numbers of genomic loci in differentiating ES cells (10 nM RA treatment for 2 days). DRB was used during culturing of cells where indicated. The x-axis corresponds to genomic locations; the y-axis corresponds to the normalized ChIP-Seq signal density. Representations of UCSC genes are shown on the bottom, in which Hox loci (E) and the other representative loci (F) are shown. RAR ChIP-Seq datasets (GSE19409) [22] were downloaded from the NCBI Short Read Archive database. (**G**) Bar charts showing relative ratios of the numbers of RAR-associated genes in indicated gene groups in differentiating ES cells. The gene groups are classified according to fold change in Lys36me2/3 levels in response to DRB: Δlog2 transformation of normalized reads/kb/million mapped (RPKM) values of each gene in DRB (+) over those in (−). Total numbers of genes in each gene group are indicated on the right side of each graph. Chi-square testing was used for calculation of P-values where indicated, *P<0.001. (**H**) Distributions of Lys36me2/3 ChIP-Seq read counts relative to RAR binding sites in ES cells in the presence or absence of DRB.
doi:10.1371/journal.pgen.1003897.g004

Figures 4E and 4F show profiles of the representative genomic regions. In these genomic profiles, we found that the level of Lys36me2 in wild-type cells was generally unchanged in response to DRB in a broad range of regions, or rather increased in some parts, while that of Lys36me3 was decreased in most regions. However, we also found that substantial levels of Lys36me3 remained in scattered regions, including some inter-genic regions. Interestingly, quite a few such regions were found in the vicinity of RAR binding sites [22], implicating a functional relationship between Lys36me3 in response to DRB and RA signaling. Indeed, the numbers of RAR-associated genes were significantly under-represented in a gene group with decreased levels of Lys36me3 in response to DRB (Figure 4G, $\Delta Log2 < -0.6$). Most strikingly, RAR binding sites showed a major peak in the Lys36me3 ChIP-Seq read density plot (Figure 4H). Additionally, in B16 cells, which express *Hoxd4* constitutively without the addition of RA, we observed only a small increase in Lys36me3 levels in response to DRB (Figure S5). These results further support our proposed relationship. Taken together, our results indicate that Lys36me2 by Ash1l and other dimethylases occurs independently of RNAPII Ser2p in a large number of genomic regions. However, whether Lys36me3 occurs independently of RNAPII Ser2p is context-dependent, and at least in a portion of genomic regions, RAR may play a substantial role for maintaining Lys36me2/3 levels.

Lys36me occurs independently of productive transcriptional elongation

In the above experiments, it is possible that past productive transcriptional elongation had left unknown traces on the transcribed chromatin, which in turn was targeted by several Lys36-methylases including Ash1l, although recruitment of the methylases is independent of RNAPII Ser2p. Moreover, it remains unclear whether the activation of the enzymatic activity of Ash1l requires the productive transcriptional elongation. Therefore, in the next experiments, to block the productive transcriptional elongation completely, we used DRB prior to administering RA. Specifically, DRB was added 1 hour before the addition of RA,